

6 Theoretical Calculation of Reduction Potentials

*Junming Ho, Michelle L. Coote,
Christopher J. Cramer, and Donald G. Truhlar*

CONTENTS

I.	Introduction	229
II.	Formal Definitions, Electrochemical Concepts, and Basic Considerations	231
	A. Ionization Potentials and Electron Affinities.....	231
	B. Standard versus Formal Potentials	232
	C. Cyclic Voltammetry	233
	D. Effects of Protonation	234
	E. Reversible and Irreversible Redox Processes.....	235
	F. Liquid Junction Potentials.....	235
	G. Reference Electrodes	236
III.	Computation of Reduction Potentials	236
	A. Gas-Phase Free Energies of Reaction	237
	1. Gibbs Free Energy and the Treatment of Nuclear Motion.....	237
	2. Electronic Energies of Atoms and Molecules.....	240
	3. Standard State of the Electron	241
	B. Free Energies of Solvation	242
	1. Absolute Potential of the Aqueous SHE.....	243
	2. Nonaqueous Systems	244
	C. Standard States	245
	D. Rates of Electron Transfer	247
IV.	Examples.....	247
	A. Aqueous Standard One-Electron Reduction Potentials of Nitroxides and Quinones...	247
	B. Chemically Irreversible Processes—Reductive Dechlorination	250
	C. Constructing a Pourbaix Diagram for the Two-Electron Reduction of <i>o</i> -Chloranil	252
V.	Concluding Remarks	255
	Acknowledgments.....	255
	References.....	255

I. INTRODUCTION

The reduction potential is a direct measure of the thermodynamic feasibility of an oxidation–reduction half reaction; and it is fundamentally important in many aspects of organic, bioorganic, and environmental chemistry, as well as in biology and materials science. The design of rational strategies for tuning the redox properties of compounds depends on understanding the key molecular features that dictate the reduction potential. As an example, in environmental chemistry, chlorinated aliphatic compounds are common environmental contaminants due to their widespread use as solvents and degreasers and are known to degrade via a reductive

dehalogenation [1,2]; the environmental persistence of these compounds has been found to correlate with their relative reduction potentials, and the computation and measurement of these quantities is therefore valuable for understanding structure–activity trends and the design of environmentally friendly derivatives of these compounds [1,3–8]. Similarly, in biochemistry, nitroxides are a class of kinetically stable free radicals that have been widely studied as potential antioxidants against reactive oxygen species, which can lead to tissue injury and even cell death; both oxidation and reduction processes involving nitroxides are biologically relevant [9–12], and the ability to predict the redox potentials of nitroxides with various substituents and those embedded in rings can help prioritize synthetic targets for potentially biologically relevant antioxidants [13,14].

Reduction potentials are most straightforwardly defined when associated with readily reversible equilibria; in such instances, they contain equivalent information to equilibrium constants or free energy changes for electrochemical half reactions. In practice, the high reactivity of many species (e.g., organic radicals) participating in electrochemical reactions or the irreversibility or mechanistic complexity of redox reactions can make the direct experimental measurement of a corresponding reduction potential difficult. For this reason, computational chemistry offers a valuable alternative to experiment for the characterization of redox reactions. The theoretical calculation of any thermochemical quantity, including free energies and therefore including reduction potentials, usually takes advantage of the Born–Oppenheimer separation of electronic and nuclear motion, which ultimately reduces the problem to three steps: (1) the calculation of molecular potential energy surfaces by electronic structure calculations; (2) the treatment of nuclear motion, for example, vibrations; and (3) statistical mechanical averaging over relevant configurations, conformations, or solvent structures. Step (3) is often carried out by classical statistical mechanics and step (2) by quasiharmonic methods, whereas step (1) generally requires more expensive quantum mechanical (QM) calculations, which can limit the accuracy of predictions if sufficiently large systems make the application of accurate QM models impractical. However, the relatively recent development of efficient quantum chemical algorithms and powerful computer architectures has facilitated the quantitatively useful study of many reactions. Because most redox processes of practical interest occur in condensed phases, the development of reliable solvation models has also been critical to progress, and both implicit and explicit solvent models are now available such that well-chosen combinations of theoretical models have the potential to be used to make quantitative predictions of electrochemical quantities like reduction potentials.

Although this chapter is concerned with thermodynamics, the reader should keep in mind that reactivity and biological activity also depend on kinetics. While kinetics is often correlated with thermodynamic descriptors such as reduction potentials, it also includes other factors whose complete discussion is beyond the scope of this chapter. Nevertheless, we will mention kinetic effects in some places because they are relevant to interpreting measurements.

There are several approaches to calculating a condensed-phase reduction potential, ranging from phenomenological or theoretically guided linear free energy relationships (LFERs) correlating reduction potentials with other computed (or experimental) observables to direct calculations of reduction potentials. When using LFERs, computed properties are again often obtained by QM electronic structure calculations. Calculated or measured properties that may be correlated with reduction potentials include ionization energies and electron affinities in the gas phase, as well as energies of the frontier molecular orbitals (e.g., the highest occupied molecular orbital), and these quantities may be regressed on solution-phase reduction potentials in order to develop a predictive equation [15–28]. LFERs are appealing because they allow for very rapid evaluation of reduction potentials, which is especially important, for example, in high-throughput screening of large databases of drug candidates. The implicit assumption of such an approach is that the errors associated with neglecting contributions to the reduction potential that do not correlate with the chosen independent variables are negligible, as are errors associated with the level of theory used to compute these variables. In practice, LFERs may work well if the compounds under consideration

are sufficiently similar to those used in the regression. The semiempirical nature of this approach means that it may be difficult to estimate the errors associated with these models, particularly when they are applied on compounds outside of the training set.

When one attempts to calculate the reduction potentials directly, without linear regression against simpler quantities, typically only the most active portion of the system, for example, the solute and perhaps the first-solvent shell, is treated explicitly by quantum mechanics. The rest of the system is treated by molecular mechanics (MM), classical electrostatics, or both (although occasionally the whole system is treated by explicit quantum mechanics). Combining quantum mechanics for a primary subsystem with MM for the rest of the system is labeled QM/MM, and if the MM subsystem is the solvent, it is an example of an explicit solvent method that requires molecular dynamics (MD) or Monte Carlo (MC) methods to ensemble average the solvent. MD and MC free energy simulations permit examination of solvent structure and reorganization [29–32]. Methods based on classical electrostatics usually replace the discrete solvent molecules by a dielectric continuum, so that the solvent and the ensemble average over solvent configurations both become implicit. QM/MM and implicit-solvent treatments are the methods of choice for the study of redox potentials in condensed-phase and biological systems because treating the entire system quantum mechanically raises the cost so much that one is usually forced to use less reliable methods or to skimp on ensemble averaging.

In this chapter, we will focus exclusively on methods based on thermodynamic cycles where solution-phase reduction Gibbs free energies are computed by combining gas-phase energetics with solvation free energies of the products and reactants. Such methods are also used extensively in solution-phase pK_a predictions [33–35] as well as in studies of other condensed-phase reactions such as free-radical polymerization [36,37].

In the following, Section II presents some formal concepts in equilibrium electrochemical thermodynamics. The Section III is concerned with the implementation of the computational protocols. The Section IV presents some worked examples.

II. FORMAL DEFINITIONS, ELECTROCHEMICAL CONCEPTS, AND BASIC CONSIDERATIONS

This section introduces some formal concepts in equilibrium electrochemical thermodynamics that are important for calculating solution-phase reduction potentials.

A. IONIZATION POTENTIALS AND ELECTRON AFFINITIES

The adiabatic ionization energy, usually called the ionization potential, is the energy required to form a molecular or atomic cation in its ground state via the loss of an electron from the ground state of the neutral system in the gas phase. The vertical ionization energy applies to the change in electronic energy upon removal of an electron from the equilibrium structure of the neutral without change in geometry, again in the gas phase. For this reason, the two quantities are identical for an atom, and for a molecule the vertical ionization energy is almost always higher than its adiabatic counterpart. The electron affinity (EA) is defined similarly to the adiabatic ionization energy, and the vertical electron attachment energy is similar to the vertical ionization energy, but these quantities refer to minus the change in energy when a neutral system gains an electron. The adiabatic quantities correspond to enthalpy changes at 0 K:



where the subscript denotes the temperature in units of kelvin.

B. STANDARD VERSUS FORMAL POTENTIALS

At the heart of electrochemical thermodynamics is the chemical potential (μ), which equals the molar Gibbs energy (G) for a pure substance and the partial molar Gibbs free energy for a component of a solution. For a species A in a solution,

$$\mu_A = \mu_A^\circ + RT \ln \left(\frac{\gamma C}{C^\circ} \right) = \mu_A^\circ + RT \ln(a) \quad (6.2)$$

where

C is the concentration

a small circle in a superscript denotes the value of a quantity in the standard state

a and γ are the activity and activity coefficient, respectively

The usual standard states in the gas phase are an ideal gas at a pressure of 1 atm or 1 bar (0.987 atm), and the usual standard states for solutes in liquid-phase solutions are ideal solutions at a concentration of 1 M (1 mol/L of solution) or 1 molal (1 mol of solute/kg of solvent). Notice that we have introduced the dimensionless activity coefficients γ_i defined by [38]

$$a_i = \gamma_i \frac{c_i}{c_i^\circ} \quad (6.2a)$$

If we apply Equation 6.2 to the reaction



where

Ox is the oxidant

Red is the reductant

the free molar energy of reaction is given by

$$\Delta G = \Delta G^\circ + RT \ln Q = \Delta G^\circ + RT \ln \left(\frac{a_{\text{Red}}}{a_{\text{Ox}}} \right) \quad (6.4)$$

where Q is the dimensionless reaction quotient. The relation between free energy and the maximum electrical work that can be performed, as expressed in terms of the electrode potential E of a half-cell [39], is

$$\Delta G = -nFE \quad (6.5)$$

where

F is the Faraday constant (96,485 C mol⁻¹)

n is the number of electrons in the half reaction

Combining this with Equation 6.4 yields the following Nernst equation [40]:

$$E = E^\circ + \frac{RT}{F} \ln \left(\frac{a_{\text{Ox}}}{a_{\text{Red}}} \right) \quad (6.6)$$

where E° is the standard electrode potential, also called the standard-state potential or the half-cell potential.

Notice that E equals E° when the activities of all species are 1. However, such standard-state conditions are often difficult to achieve in practice, and standard-state potentials are often replaced by *formal potentials*, $E^{\circ'}$. Formal potentials are sometimes called conditional potentials to denote that they apply under specified conditions rather than under standard conditions [38]. Specifically, this quantity is the measured potential of the half-cell when the ratio of the total concentrations of oxidized and reduced species is unity and other specified substances (e.g., proton) are present at designated concentrations. For example, they can be defined to correspond to the half-cell potentials when the *concentration* quotients (Q_c) in the Nernst equation equal 1:

$$E = E^{\circ'} + \frac{RT}{F} \ln Q_c = E^{\circ'} + \frac{RT}{F} \ln \left(\frac{C_{\text{Ox}}}{C_{\text{Red}}} \right) \quad (6.7)$$

Then the formal potential ($E^{\circ'}$) is related to the standard reduction potential (E°) as follows:

$$E^{\circ'} = E^\circ + \frac{RT}{F} \ln \left(\frac{\gamma_{\text{Ox}}}{\gamma_{\text{Red}}} \right) \quad (6.8)$$

For example, the absolute potential of the *normal hydrogen electrode* is based on a concentration of the proton equal to 1 mol L⁻¹ and is therefore a formal potential. This may be corrected to give the absolute potential of the standard hydrogen electrode (SHE) by taking into account the activity coefficient for a 1 mol L⁻¹ solution of [H⁺] in water, which has been estimated to be 0.8 [41]:

$$E_{\text{SHE}}^\circ = E_{\text{NHE}} - \frac{RT}{F} \ln(\gamma_{\text{H}^+}) = E_{\text{NHE}} + 0.006 \text{ V} \quad (6.9)$$

In this particular instance, activity effects account for only a small change (6 mV) in the potential [42]. As an example of a more extreme case, the formal potential of the Fe³⁺/Fe²⁺ couple varies from 0.53 to 0.7 V in 10 and 1 mol L⁻¹ HCl solutions, respectively [43].

Typically, experimental standard reduction potentials are obtained by assuming a functional form that models the dependence of the potential on ionic strength. A series of formal potential measurements is then carried out at different values of ionic strength, and they are extrapolated to zero ionic strength where the activity coefficients approach unity [43].

C. CYCLIC VOLTAMMETRY

Cyclic voltammetry is commonly used in the determination of formal potentials, which may be extracted directly from a fully reversible cyclic voltammogram as the average (*midpoint*) of the anodic and cathodic peak potentials, E_{pa} and E_{pc} , or from the half-wave potential of a sigmoid curve in steady-state voltammetry [43], to give a half-wave or midpoint potential, $E_{1/2}$. Because the measured half-wave potential is affected by diffusion (a nonthermodynamic effect), it is related to the formal potential by

$$E_{1/2} = \frac{E_{\text{pc}} + E_{\text{pa}}}{2} = E^{\circ'} + \frac{RT}{2nF} \ln \left(\frac{D_{\text{Red}}}{D_{\text{Ox}}} \right) \quad (6.10)$$

where D_{Ox} is the diffusion coefficient of Ox. When the diffusion coefficients of the oxidized and reduced species are very similar, the half-wave potential provides a good approximation to the formal potential.

D. EFFECTS OF PROTONATION

In aqueous solution, thermodynamically favored proton transfer is usually rapid, and electrochemical measurements usually give reduction potentials for half reactions that include any thermodynamically favorable proton addition or loss. As such, an n -electron, m -proton half reaction can be represented in two possible ways:



with corresponding standard reduction potentials denoted $E^\circ(\text{Ox}/\text{Ox}^{n-})$ and $E^\circ(\text{Ox}, m\text{H}^+/\text{H}_m\text{Ox}^{(n-m)-})$, respectively. The potential for the latter equation is directly dependent on pH and is equal to the formal potential $E^{\circ'}(\text{Ox}, m\text{H}^+/\text{H}_m\text{Ox}^{(n-m)-})$ when the concentrations of all species are 1 mol L⁻¹:

$$E = E^{\circ'} + \frac{RT}{nF} \ln \frac{[\text{Ox}][\text{H}^+]^m}{[\text{H}_m\text{Ox}]} = E^{\circ'} + \frac{RT}{nF} \ln \frac{[\text{Ox}]}{[\text{H}_m\text{Ox}]} - 2.303 \frac{RT}{F} \left(\frac{m}{n} \right) \text{pH} \quad (6.11c)$$

By monitoring how this cell potential varies with pH, it is possible to determine the electron–proton stoichiometry (m/n) of the electrochemical measurement. For example, consider quinones and their derivatives, which are electroactive organic compounds that play a vital role in a number of biochemical processes. These compounds can undergo either a two-electron reduction (Ox/Ox^{2-}), a two-electron–one-proton reduction ($\text{Ox}, \text{H}^+/\text{HOx}^-$), or a two-electron–two-proton reduction ($\text{Ox}, 2\text{H}^+/\text{H}_2\text{Ox}$), depending on the pH of the solution [44]. In Section IV.C, we illustrate how one constructs an E versus pH diagram, which is called a Pourbaix diagram [45–47] and is analogous to a chemical speciation plot or predominance zone diagram determined by pH.

A measured formal potential is a good approximation to the standard reduction potential only when activity and kinetic effects associated with chemical reaction(s) are relatively minor. Where this is not the case, explicit treatment of these effects should be included in the calculations, or comparisons should be made with other experimental potentials that correspond more closely to infinite dilution and to thermodynamic control.

Consider the reduction of nitroxide radicals in aqueous solution in Figure 6.1.

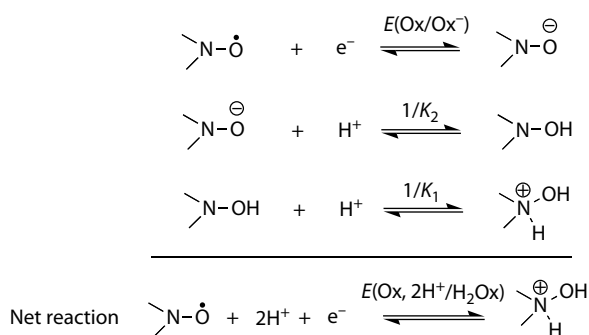


FIGURE 6.1 The microspecies present in the one-electron reduction of a nitroxide radical in aqueous solution.

The measured half-wave potential $E_{1/2}$ is related to the formal potential for the one-electron–two-proton ($1e, 2H^+$) transfer reaction as follows [48,49]:

$$E_{1/2} = E^{o'}(\text{Ox}, 2\text{H}^+/\text{H}_2\text{Ox}^+) + \frac{RT}{F} \ln(K_1 K_2 + K_1[\text{H}^+] + [\text{H}^+]^2) \quad (6.12)$$

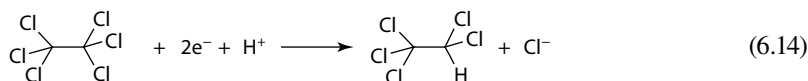
where K_1 and K_2 are the equilibrium constants associated with the protonation steps. In previous work, it was found that explicit consideration of the prototropic equilibria was necessary to obtain good agreement with the experimental half-wave potentials [14]. In some cases, the experimental potential corresponds to that for a one-electron ($1e$) transfer $E^{o'}(\text{Ox}/\text{Ox}^-)$, and this is related to the formal potential of the ($1e, 2\text{H}^+$) reduction potential $E^{o'}(\text{Ox}, 2\text{H}^+/\text{H}_2\text{Ox}^+)$ by

$$E^{o'}(\text{Ox}/\text{Ox}^-) = E^{o'}(\text{Ox}, 2\text{H}^+/\text{H}_2\text{Ox}^+) + \frac{RT}{F} \ln(K_1 K_2) \quad (6.13)$$

E. REVERSIBLE AND IRREVERSIBLE REDOX PROCESSES

Occasionally, half-wave potentials are also reported for quasi-reversible cyclic voltammetry experiments with a back wave partially present; however, the reader should note that these are usually estimated values and therefore may not be well suited for quantitative comparisons. It is impossible to extract $E_{1/2}$ from completely irreversible processes (no back wave) because of kinetic control of the current such that the Nernst equilibrium is established less quickly than the change in potential or because there are fast follow-up (side) reactions consuming the pertinent species.

There are instances where the transfer of an electron to or from a neutral precursor leaves the resulting radical ion in an electronic ground state that is dissociative [1,50]. (The former process is called dissociative attachment [51], and the latter is called dissociative ionization [52].) Following the electron-transfer event, which is rapid on the time scale of nuclear motion, the ion relaxes along the dissociative coordinate, leading to the scission of one or more bonds. Typically, the energetics associated with this fragmentation are such that the electron-transfer event is effectively irreversible. Depending on whether the ion lives long enough to be reoxidized/reduced on the return sweep, the back wave may be only partially present or completely absent in a cyclic voltammogram, in which case it is not possible to extract a half-wave potential. An example of such a *chemically irreversible* process is the reductive dehalogenation of haloalkanes. For such processes, the equilibrium potential may alternatively be defined as the Gibbs free energy associated with the overall process, which in this case is



F. LIQUID JUNCTION POTENTIALS

The liquid junction potential arises whenever solutions with two different compositions come into contact. Its magnitude depends on the relative concentrations of the various ions at the boundary and on their relative mobilities. These potentials may be significant in cases where the solvent system changes across a junction (e.g., from acetonitrile or dimethyl formamide [DMF] on one side to aqueous on the other). The liquid junction potentials of a number of dissimilar solvent junctions have been determined to range from 10 to 200 mV, depending on the junction [53].

G. REFERENCE ELECTRODES

The conventional reference electrode for aqueous systems is the SHE, which has been assigned a potential of zero in experimental measurements. In theoretical calculations, the *absolute* (rather than relative) reduction potentials are often computed, and knowledge of the absolute potential of the SHE is essential for comparing computations with experiment. A schematic of a cell with the aqueous SHE as reference and an Ox/Red couple in solvent S is as follows:



In this equation, the SHE is the anode (where oxidation takes place, on the left), and the Ox/Red couple is the cathode (where reduction takes place, on the right). The vertical lines indicate phase boundaries. The cell voltage ($E_{\text{Cathode}} - E_{\text{Anode}}$) is given by Equation 6.16 where $E_{\text{Ox/Red}}^\circ$ is the standard potential of the Ox/Red couple (see Equation 6.6) and E_j is the liquid junction potential between the aqueous SHE and the solvent/electrolyte containing Ox and Red:

$$E_{\text{cell}} = E_{\text{Ox/Red}} - E_{\text{SHE}}^\circ + E_j = E_{\text{Ox/Red}}^\circ - E_{\text{SHE}}^\circ + \frac{RT}{F} \ln \left(\frac{a_{\text{Ox}}}{a_{\text{Red}}} \right) + E_j \quad (6.16)$$

If all species are in their respective standard states, with the activity (or concentration, as an estimate for activity) equal to 1 mol L⁻¹ for solutions and fugacity (or pressure, as an estimate for fugacity) equal to 1 bar for gases, then Equation 6.16 simplifies into

$$E_{\text{cell}} = E_{\text{Ox/Red}}^\circ - E_{\text{SHE}}^\circ + E_j \quad (6.17)$$

Since the physical setup of an SHE is somewhat cumbersome, reduction potentials are often referenced to other electrodes. In laboratory measurements, a secondary reference electrode whose potential versus the SHE(aq) is well known is usually used. Examples include the (KCl) saturated calomel electrode (SCE) and the saturated silver/silver chloride electrode; the presence of saturated KCl in these electrodes leads to sharply reduced values of E_j . As such, in comparing with experiment, it is also important to examine the details of the experimental measurement to ascertain whether a correction for E_j is necessary in theoretical calculations. The conversion constants between different electrodes in aqueous solvents have been measured [54], and these may be used to convert reduction potentials that are referenced to SHE to other reference electrodes. For example, the potential of the SCE is 0.244 V relative to the SHE at 298 K in aqueous solution. Therefore, to convert values based on SHE to SCE, one needs to subtract 0.244 V.

III. COMPUTATION OF REDUCTION POTENTIALS

As indicated in Equations 6.4 and 6.5, the standard-state Gibbs free energy change for a half reaction is the quantity required for computing a standard reduction potential. Since experimental reduction potentials are not measured in isolation but are instead measured relative to the potential of a reference electrode, theoretical calculations of reduction potentials are typically carried out either for a half-cell reaction (Figure 6.2, cycle A) with the subtraction of the reduction potential of the reference electrode (e.g., SHE) or on a full-cell reaction (Figure 6.2, cycle B). In Figure 6.2 we have introduced the general notation ΔG_s° for a standard-state free energy of solvation, which is the free energy change upon transfer from the gas phase (sometimes called *air* in the transfer literature) to the liquid solution.

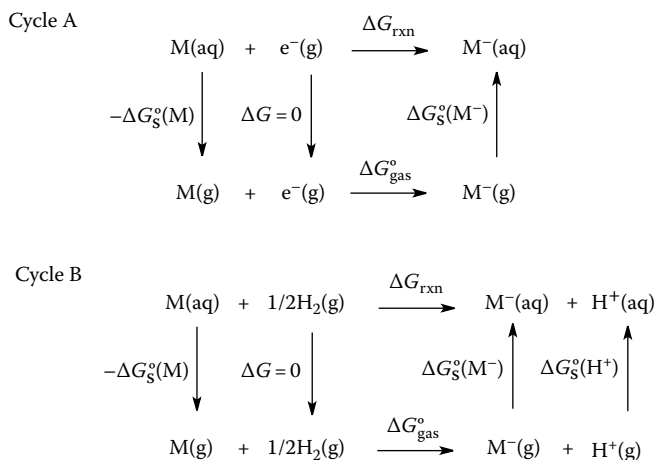


FIGURE 6.2 Thermodynamic cycles for calculating an absolute and relative reduction potential.

The corresponding reduction potentials are

$$E_{\text{cell}} = \frac{-\Delta G_{\text{rxn}}(\text{A})}{nF} - E_{\text{SHE}} \quad (\text{cycle A}) \quad (6.18)$$

and

$$E_{\text{cell}} = \frac{-\Delta G_{\text{rxn}}(\text{B})}{nF} \quad (\text{cycle B}) \quad (6.19)$$

In principle, both cycles yield the same result. However, cycle B effectively uses calculated values of E_{SHE} and $\Delta G_{\text{S}}^{\circ}(\text{H}^+)$, whereas cycle A effectively uses empirical (accurate) values. Thus, cycle A is simpler, and in this cycle, the key ingredients for the calculation of a reduction potential are the gas-phase Gibbs free energy of reaction and the free energies of solvation of the reagents, that is, of the reactants and products.

A. GAS-PHASE FREE ENERGIES OF REACTION

1. Gibbs Free Energy and the Treatment of Nuclear Motion

The Gibbs energy change of the gas-phase reaction shown in cycle A is simply the EA of M, EA(M), plus the thermal contribution to the Gibbs free energy (ΔG_{therm}) of M^- less that of M:

$$\begin{aligned}
 \Delta G_{\text{gas}}^{\circ} &= G^{\circ}(\text{M}^-) - G^{\circ}(\text{M}) \\
 &= [U_{\text{e}}(\text{M}^-) + \text{ZPE}(\text{M}^-) + \Delta G_{\text{therm}}(\text{M}^-)] - [U_{\text{e}}(\text{M}) + \text{ZPE}(\text{M}) + \Delta G_{\text{therm}}(\text{M})] \\
 &= -\text{EA}(\text{M}) + [\Delta G_{\text{therm}}(\text{M}^-) - \Delta G_{\text{therm}}(\text{M})] = -\text{EA}(\text{M}) + \Delta \Delta G_{\text{therm}}
 \end{aligned} \quad (6.20)$$

where

U_{e} denotes the Born–Oppenheimer equilibrium potential energy

ZPE denotes the vibrational zero point energy

ΔG_{therm} denotes the thermal contribution to the free energy, that is, the part that vanishes at 0 K

The thermal contribution includes the free energy due to multiple conformations (if present), rotations, and vibrational and electronic excitation. Note that the change in ZPE is included in the EA. We have neglected nuclear spin considerations, since the effect of nuclear spin cancels out in almost all cases, the main exception being the H₂ molecule.

It is useful to introduce the enthalpy at 0 K, which is labeled H_0 . Then

$$H_0 = U_e + \text{ZPE} \quad (6.21a)$$

and Equation 6.20 becomes

$$\Delta G_{\text{gas}}^\circ = H_0(M^-) + \Delta G_{\text{therm}}(M^-) - H_0(M) - \Delta G_{\text{therm}}(M) \quad (6.21b)$$

If the conformations, geometries, and vibrational frequencies of the charged molecule are very similar to those of the neutral and neither has low-lying electronically excited states, then the thermal correction to the Gibbs energy of M^- and M is likely to be similar and one could roughly estimate $\Delta G_{\text{gas}}^\circ$ as approximately equal to EA(M). In some cases however, the gain (or loss) of an electron can result in significant changes to the electronic structure of a molecule (e.g., quinones acquire an aromatic ring structure upon the gain of two electrons), and this approximation becomes unreliable. In such situations, the thermal corrections are sometimes calculated by assuming ideal gas behavior and the rigid-rotor harmonic oscillator approximation, to arrive at analytic expressions for the molecular partition function (\tilde{Q}), from which one can calculate the entropy (S), and the thermal contributions to the enthalpy (ΔH_{therm}) and the Gibbs free energy (ΔG_{therm}), which are evaluated from the following expressions:

$$\begin{aligned} S &= R \left(\ln \tilde{Q} + T \left(\frac{\partial \ln \tilde{Q}}{\partial T} \right)_V \right) \\ \Delta H_{\text{therm}} &= RT^2 \left(\frac{\partial \ln \tilde{Q}}{\partial T} \right)_V + RT \\ \Delta G_{\text{therm}} &= \Delta H_{\text{therm}} - TS \end{aligned} \quad (6.22)$$

where \tilde{Q} is the molecular partition function with zero of energy at the ground state and the equivalent expression for the Gibbs free energy in terms of \tilde{Q} is

$$G = U_e + \text{ZPE} + PV - RT \ln \tilde{Q} \quad (6.23)$$

Furthermore, if one assumes that there is only one conformation and negligible coupling between electronic excitation, vibrations, and rotations, the molecular partition function can be separated into a product of partition functions associated with the translational, rotational, vibrational, and electronic motions:

$$\tilde{Q} = q_{\text{trans}} q_{\text{rot}} q_{\text{vib}} q_{\text{elec}} \quad (6.24)$$

If we assume separability, the electronic partition function is

$$q_{\text{elec}} = \omega_1 + \sum_{i=2}^{\infty} \omega_i \exp \left(\frac{-\epsilon_i}{k_B T} \right) \quad (6.25)$$

where

ϵ_i is the electronic energy (including nuclear repulsion but not vibrational energy) of level i

ω_i is the degeneracy of that level

When the first electronic excitation is thermally inaccessible at room temperature, the electronic partition is well approximated by the degeneracy associated with the electronic ground state:

$$q_{\text{elec}} = \omega_1 \quad (6.26)$$

For monatomic species, if the total electronic angular momentum associated with electronic state i is J_i , we have $\omega_i = 2J_i + 1$. For example, the ground state of a halogen atom is $^2P_{3/2}$ with $J_1 = 3/2$, so $\omega_1 = 4$, and the first excited state is $^2P_{1/2}$ with $J_2 = 1/2$ and $\omega_2 = 2$. Based on Equation 6.25 and the excitation energy of 0.109 eV of the first electronically excited state, the electronic partition function for chlorine atom at 298 K is therefore

$$q_{\text{elec}} = 4 + 2e^{-4.2} = 4.03 \quad (6.27a)$$

Higher excited states make a negligible contribution in this case.

The vibrational partition function is usually treated by the harmonic oscillator approximation or by a quasiharmonic approximation in which one uses the harmonic oscillator formulas but scales the frequencies [55–57] to account for anharmonicity (and for systematic deficiencies of the electronic structure method used to calculate the frequencies).

The rotational partition function is usually treated classically.

For molecules where there are multiple conformers that are close in energy to the lowest-energy structure, the conformational flexibility contributes to the G_{therm} . If we again make a separable approximation, we can include this by putting another factor in Equation 6.24, yielding

$$\tilde{Q} = q_{\text{trans}} q_{\text{rot}} q_{\text{vib}} q_{\text{elec}} q_{\text{conf}} \quad (6.27b)$$

$$q_{\text{conf}} = \sum_{j=1}^{N_{\text{conf}}} \exp\left(\frac{-\Delta U_j}{k_B T}\right) \quad (6.27c)$$

where ΔU_j is the potential energy difference of conformation j from the lowest one and the conformational partition function is summed over all the conformational space of the molecule, which is equivalent to performing a Boltzmann average over the Gibbs free energies of all the conformers. A much better approximation is to use Equation 6.24—or a more accurate analog with less separability approximations—to calculate a free energy G_j for each conformer. Then the free energy including all conformers is

$$G = -RT \ln \sum_j \exp\left(\frac{-G_j}{k_B T}\right) \quad (6.27d)$$

One should only include distinguishable conformers. However, even the number of distinguishable conformers grows rapidly with molecule size for chain molecules. For example, n -heptane has 59 distinguishable conformations [58]. Glucose has 2916 potential conformations [59]. Even the approximation of Equation 6.27d is far from realistic, though, if the barriers separating the conformers are not all high compared to $k_B T$, both because the contributions of any one conformer are no longer independent and because the individual contributions differ from their harmonic values. If the barriers are low, the system must be treated as having one or more internal rotations. A theoretical formalism, based on internal coordinates and including intermode coupling, is available [60].

In practice, a full conformational search typically involves at least 3^N geometry optimizations where N is the number of rotatable bonds in the molecule that yield distinguishable structures (e.g., the C-3 to C-4 torsion in 1-butanol does not yield distinguishable structures). Additional considerations apply if one must consider ring isomerism as well as torsional isomerism. Therefore, a full conformational search is usually restricted to molecules with $N \leq 5$. It is worth noting that a rough approximate upper bound on the effect of considering higher conformers is given by the case where there are N_{conf} conformers with energies, structures, and frequencies identical to those of the lowest-energy structure; then the error associated with not including the conformational partition function is $RT \ln(N_{\text{conf}})$.

A variety of methods such as simulated annealing [61], MC methods [62], and an energy-directed tree search algorithm [63] have been developed for locating the lowest-energy conformer without having to sample the entire conformational space of the molecule. In principle, one should rank the conformers in terms of their Gibbs free energies as in Equation 6.23; however, this entails relatively expensive Hessian calculations, and in practice, the conformers are usually ranked in terms of their electronic energies (U_e). As a precaution, one could, at the end of the search, perform Hessian calculations only on conformers that are within some energy difference from the lowest-energy structure and rerank the conformers in terms of their Gibbs energies.

The expressions for the partition functions as derived from the ideal gas, rigid-rotor harmonic oscillator approximation can be found in standard textbooks [64] and will not be presented here. A discussion of the potential sources of error in the application of these partition functions (e.g., breakdown of the harmonic oscillator approximation) and the errors that could arise from the assumptions used to derive them has been discussed elsewhere [65,66]. These treatments assume that the torsions are separable and may be identified with specific normal modes. When this is not the case, one must use the internal-coordinate nonseparable treatment mentioned earlier [60].

Having laid out the key ingredients for calculating a gas-phase Gibbs free energy, we now discuss possible levels of theory for calculating geometries, Born–Oppenheimer (electronic) energies, and free energies.

Geometries are often calculated at lower levels of theory such as density functional theory (DFT) with a small basis set that can predict equilibrium geometries and vibrational frequencies (when scaled by appropriate scale factors [56,57,60]) reasonably well but is not usually sufficiently accurate for reaction energies. However, it is also usually possible to calculate geometries at the same level as reasonably reliable energies if one uses DFT with a modern density functional and a good basis set.

2. Electronic Energies of Atoms and Molecules

Chemically accurate (errors of 5 kJ mol^{-1} or less) electronic energies of reaction can usually be achieved for small- and moderate-sized systems provided that electronic energies are calculated at high levels of theory, for example, CCSD(T) or QCISD(T), with very large one-electron basis sets incorporating high angular momentum basis functions. Here CC denotes coupled cluster theory, QCI denotes quadratic configuration interaction, SD denotes the inclusion of single and double excitations, and (T) denotes a quasiperturbative treatment of connected triple excitations [67]. One difficulty with electronic wave function theory (WFT) methods of this sort is the very slow convergence of the energies with respect to the size of the one-electron basis set. Furthermore, a CCSD(T) calculation formally scales as the seventh power of the number of atoms in the system [67] and is therefore restricted to relatively small molecular systems. Popular alternatives to large-basis-set CCSD(T) calculations are composite methods that have been designed to approximate high-level-correlated calculations using a series of lower cost calculations in conjunction with additivity and/or extrapolation routines. The Gaussian- n (e.g., G4 [68], G3 [69], G3(MP2) [70], and G3(MP2)-RAD [71,72]) methods with high-level corrections, multicoefficient correlation methods [73–82], the correlation-consistent composite approach [83,84], and CBS- X (e.g., where X is QB3 [85]) are examples of such methods. These methods involve some degree of empirical parameterization and are practical for medium-sized systems. By comparison, the W_n ($n = 1-4$) methods [86–89] have been designed to

compute thermochemical properties with even higher accuracy (ca. 1 kJ mol⁻¹), without empirical parameterization, but are also considerably more expensive and therefore limited to relatively small systems. For larger systems where even composite methods become computationally expensive, one could employ an ONIOM approximation [90,91] where the chemical system is partitioned into layers. The innermost layer is usually defined by the reaction center and its nearby substituents so that the chemistry of the reaction is modeled accurately. This layer is treated at the highest level of theory. The subsequent layer(s) are then treated at lower levels of theories. As an example, this approach has been successfully used to approximate the G3(MP2)-RAD calculations for a test set of 112 different radical reactions with a mean absolute deviation of 1.2 kJ mol⁻¹ [92]. There are a large number of other shortcuts and “tricks of the trade,” for example, basis-set extrapolation [93–96] to ameliorate the aforementioned slow convergence, but these are too numerous to mention.

An important alternative to WFT is DFT. Here the computational work scales as N_{atom}^3 or N_{atom}^4 rather than N_{atom}^7 , where N_{atom} is the number of atoms in the system, but the accuracy depends on the quality of the exchange–correlation functional [97]. This quality is improving rapidly [98].

We next address relativistic effects, which begin to be energetically important at the level of chemical accuracy near the end of the first transition-metal series. There are two kinds of relativistic effects: (1) scalar relativistic effects and (2) spin–orbit coupling [99]. Scalar relativistic effects are most simply handled by replacing the core electrons with appropriate effective core potentials [100–105]; however, the accuracy can be low [106]. If all electrons are to be treated, the most rigorous approach makes use of the four-component Dirac spinor operator. More efficient approaches are based on two-component spinors; such methods can be derived from the four-component formulation through various transformations that lead either to the Douglas–Kroll–Hess Hamiltonian [107–109] or the zero-order-regular approximation [110]. Additional reduction to a one-component formulation yields the spin–orbit operator in its usual form and also a spin–spin interaction term [111].

Spin–orbit effects, associated with the coupling of spin and orbital angular momenta in a relativistic framework, are sometimes neglected in electronic structure calculations that make use of basis sets including relativistic pseudopotentials [99]. Rather, only *scalar* relativistic effects are included and computed energies represent averages over spin–orbit states, if they exist. Spin–orbit effects *can* be included through either perturbation theory or variational methods without sacrificing the simplicity of one-component computational models. When the relevant transition-metal compounds may be viewed as substantially ionic in character, a particularly simple approach is to estimate spin–orbit effects on standard reduction potentials by assuming the same spin–orbit coupling in the complexes as that for the bare ions, where the latter are usually available from experiment.

3. Standard State of the Electron

In calculating ionization energies and electron attachment energies at nonzero temperatures or when calculating the free energy of reaction of processes like Equation 6.3, one needs to take into account the Gibbs free energy of the electron. There are two thermochemical conventions concerning the thermodynamics of the electron: (1) the electron convention (EC) and (2) the ion convention (IC). There are various literature reports giving slightly different calculated reduction potentials depending on which thermochemical convention of the electron is used. However, this should not be the case, and it originates from confusion regarding the definition of the zero of energy in the two conventions. An important point is that the Gibbs free energy obtained from a particular convention must be compatible with the quantum chemical calculation, that is, they need to have the same zero of energy. In quantum chemistry, it is convenient to define a zero of energy, at least temporarily, as corresponding to all nuclei and electrons being infinitely separated and at rest. With regard to the zero of energy for the free electron, the two conventions primarily differ in their definition of the formation enthalpy of the electron. The EC treats the reference state for electrons in the same way as for elements, that is, the enthalpy of formation is defined to be zero at all temperatures, $\Delta_f H_{\text{T}}^{\circ}(\text{e}^-) = 0$. On the other hand, the IC defines the standard enthalpy of formation of the electron to be equal to

TABLE 6.1
Thermodynamics of the Electron under the Various Thermochemical Conventions^a

	EC–B	IC (Bartmess)	IC–B	EC/IC–FD
$\Delta_f H_{298}^\circ$	0	0	6.197	0
$\Delta_f G_{298}^\circ$	0	(0) ^b	0	0
S_{298}°	20.979	(0) ^b	20.979	22.734
$[H_{298}^\circ - H_0^\circ]$	6.197	0	6.197	3.146
G_{298}°	-0.058	(0) ^b	-0.058	-3.632

EC, electron convention; IC, ion convention; B, Boltzmann statistics; FD, Fermi–Dirac statistics.

^a Enthalpies and free energies in kJ mol⁻¹, entropies in J mol⁻¹ K⁻¹.

^b Defined values [114].

its integrated heat capacity at all temperatures [112,113]. Accordingly, under the two conventions, the enthalpy of formation of ions differs by the integrated heat capacity of the electron; the actual value depends on the statistical formalism used to treat the electron. Using Boltzmann statistics and the ideal gas model, the Gibbs energy of the electron is 0 kJ mol⁻¹ at 298 K. However, since electrons are fermions, Fermi–Dirac statistics are more appropriate, and this yields a Gibbs energy of -3.6 kJ mol⁻¹ at 298 K. Contrary to the earlier report by Bartmess [114], these values are the same under both conventions and the thermochemistry of the electron is summarized in Table 6.1. In the calculation of reduction potentials, it makes no difference which formalism or convention is used as long as these are used consistently for both the half-cell and the reference electrode.

B. FREE ENERGIES OF SOLVATION

Continuum solvation models [115–118] have been designed to make accurate predictions of free energies of solvation. Free energies of solvation can then be combined with the gas-phase Gibbs energies in Equations 6.20 and 6.21 to obtain the Gibbs free energy of reaction in solution.

In continuum solvation models, the solute is encapsulated in a molecular-shaped cavity embedded in a dielectric continuum. The solute is acted on by a reaction field, which is the field exerted on the solute by the polarized dielectric continuum, and the polarization of the solute by this field is calculated via the Poisson equation for a nonhomogeneous dielectric medium (the nonhomogeneous formulation [119] is required because ϵ is unity inside the cavity—because polarization is treated explicitly—but not unity outside the cavity where it is given the value of the solvent's bulk dielectric constant). The reaction field is used to calculate the bulk-electrostatic contribution, which is then combined with the non-bulk-electrostatic terms to yield the solvation free energy. There are two contributions to the non-bulk electrostatics. One is the deviation of the true electrostatics from the electrostatics calculated using the bulk dielectric constant. The other is the nonelectrostatic portion of the solvation free energy. Some continuum solvent models such as the polarized continuum models (PCM, e.g., [IEF]-PCM [120] (IEF = integral equation formalism) and CPCM [121,122]) model the non-bulk-electrostatic and bulk-electrostatic terms independently; such models are called [123] type 3 models. Such models are less accurate than type 4 models [49,118,123–131], which are models in which the non-bulk-electrostatic terms are adjusted to be consistent with a particular choice of the cavity boundary. This adjustment is necessary because that boundary is intrinsically arbitrary, but the bulk-electrostatic contribution is very sensitive to it. The most accurate of the type 4 continuum solvation models are SM8 [129], SM8AD [128], and solvation model based on density (SMD) [127]. (These are sometimes called SM_x models where *x* specifies which one.) The conductor-like screening model for real solvents (COSMO-RS) [132,133] adopts a different strategy in which a conductor-like screening calculation is performed on a molecule to generate a set of screening charges on the molecular cavity.

The distribution of these charges forms a unique *electrostatic fingerprint* (called the σ -profile) that is characteristic of that molecule. The solvation free energy is then evaluated from a statistical mechanical procedure involving the interaction of the screening charges of the solute and those of the solvent. The COSMO-RS model has good accuracy (similar to the SM x models), at least for neutral solutes.

The coupling of the solute to the solvent is directly related to Gibbs free energy change associated with the transfer of a particle in the gas phase to the solvent in a process in which the concentration in moles per liter does not change [134]. Therefore, it is sometimes convenient to use a standard state where the solute concentration in both phases is 1 mol L⁻¹, and this standard state is denoted by “*” in ΔG_S^* , to distinguish it from ΔG_S° , which corresponds to a gas-phase partial pressure of the solute of 1 atm or 1 bar.

We note that when metal complexes have open coordination sites, it is generally inaccurate to assume that a continuum solvation approach will accurately reflect the interactions of the metal with the “missing” first solvation shell. In principle, first-shell solvent molecules could be regarded as ligands that are explicitly included in the atomistic model. Indeed, for small, highly charged ions, it may be necessary for highest accuracy to include explicitly not only the first solvation shell but also the second [135,136]. However, inclusion of even the first shell raises questions about conformational averaging, and the best practical way to address these questions has not yet been convincingly demonstrated.

The option of adding explicit solvent is more general than just filling open coordination sites. It has been concluded that continuum solvent models become quantitatively inaccurate near highly concentrated regions of charge [33,130]. Therefore, it was recommended that one should add a single explicit water molecule to any anion containing three or fewer atoms, to any anion with one or more oxygen atoms bearing a more negative partial atomic charge than the partial atomic charge on oxygen in water, and to any (substituted or unsubstituted) ammonium or oxonium ion [130].

Next, we comment on the issue of molecular geometry. Many solvation calculations use the gas-phase geometry in both phases. This is often reasonable because the difference in solvation energies calculated with gas-phase geometries and liquid-phase geometries is often less than other uncertainties in the calculations. However, it is safer to optimize the geometry separately in each phase. In cases where the conformational or other structural change associated with solvation is large, one can include this contribution to the solvation free energy computed on the solution-phase optimized geometry as follows:

$$\Delta G_S \cong \Delta G_S(\text{soln geom}) + E_{\text{gas}}(\text{soln geom}) - E_{\text{gas}}(\text{gas geom}) \quad (6.28)$$

Discussions of the use of gas-phase and solution-phase frequencies are given elsewhere [137,138].

1. Absolute Potential of the Aqueous SHE

In calculating free energies of solvation of ionic species (with charge $\pm z$), a distinction is made between the absolute or intrinsic free energy of solvation and the real free energy of solvation, where the latter includes the contribution associated with the surface potential (χ) of the solvent [139]. The surface potential of water is controversial, and a rather large scatter of values, differing by more than 1 eV, has been reported [139–143]. The choice of χ directly affects the real solvation free energy of the proton and therefore also the value of E_{SHE} , which is determined by the cycle in [Figure 6.3](#):

$$E_{\text{SHE}} = \frac{-\Delta G_{\text{rxn}}}{F} \quad (6.29a)$$

$$-\Delta G_{\text{rxn}} = \Delta G_{\text{ion}}^\circ + \Delta G_{\text{atom}}^\circ + \Delta G_S^\circ(\text{H}^+) = \Delta_f G^\circ(\text{H}^+) + \Delta G_S^\circ(\text{H}^+) \quad (6.29b)$$

At present, the E_{SHE} values of 4.28 and 4.42 V are most commonly used; these are derived from values of $\Delta G_S^*(\text{H}^+)$ of -1112.5 [144,145] and -1098.9 kJ mol⁻¹ [140], respectively, in conjunction

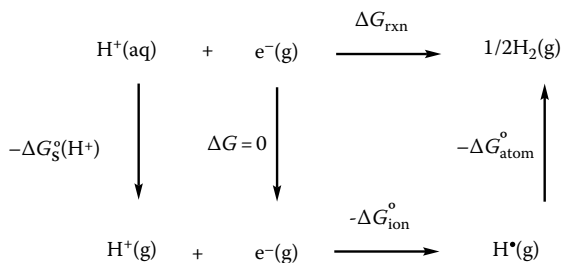


FIGURE 6.3 Thermodynamic cycle for the SHE.

with a value of $\Delta_{\text{f}}G^{\circ}(\text{H}^+)$ of 1517.0 kJ mol⁻¹. The reader should note that the values of the two terms in Equation 6.29b depend on the choice of statistical formalism used to treat the electron, and the preceding values are based on Boltzmann statistics. The corresponding $\Delta G_{\text{S}}^*(\text{H}^+)$ and $\Delta_{\text{f}}G^{\circ}(\text{H}^+)$ values based on Fermi–Dirac statistics are -1108.9 [42], -1095.3, and 1513.3 kJ mol⁻¹ [114]. The quantity $\Delta G_{\text{S}}^*(\text{H}^+)$ is positively shifted by 3.6 kJ mol⁻¹, and $\Delta_{\text{f}}G^{\circ}(\text{H}^+)$ is negatively shifted by the same amount; therefore, the value of E_{SHE} is independent of convention.

The E_{SHE} value of 4.42 V includes an estimate of the contribution due to the surface potential of water. More recent experimental estimates of E_{SHE} (4.05, 4.11, and 4.21 V) [146–148] derived from nanocalorimetric measurements have been reported; however, the uncertainty associated with this technique is still relatively large. Because the total charge is conserved in a reaction, the contribution due to the surface potential cancels out in a chemically balanced chemical reaction that occurs in a single phase. As such, where calculation of equilibrium reduction potentials involving a single phase is concerned, it should not matter whether the contribution from surface potential is included in the solvation free energy, as long as this is done consistently for all reacting species and products. This raises the question as to whether continuum solvent models are designed to predict real or absolute solvation free energies. Continuum solvent models generally contain parameters (e.g., atomic radii used to construct the molecular cavity) that have been optimized to reproduce experimental solvation free energies. However, the experimental solvation free energies of ionic solutes are indirectly obtained via thermochemical cycles involving, for example, the solvation free energy of the proton, aqueous $\text{p}K_{\text{a}}$ values, and gas-phase reaction energies. Accordingly, the E_{SHE} values that should be used with a continuum model are those that are based on a consistent $\Delta G_{\text{S}}(\text{H}^+)$.

Table 6.2 provides an overview of several continuum solvent models typically used in aqueous calculations, the $\Delta G_{\text{S}}(\text{H}^+)$ upon which they are based, and examples of the levels of theory for which they have been most extensively benchmarked. As shown, some continuum solvent models such as the (C)PCM-UAHF and (C)PCM-UAKS models, where UAHF denotes the use of united-atom parameters optimized for Hartree-Fock calculations, and UAKS denotes the use of united-atom parameters optimized for Kohn-Sham calculations, are based on $\Delta G_{\text{S}}^*(\text{H}^+)$ values that are slightly different from those used to derive the E_{SHE} values of 4.28 and 4.42 V. In such cases, where the difference is significant, one could adjust the value of the E_{SHE} to make it compatible with the continuum solvent model as shown in Table 6.2. The COSMO-RS model was parameterized using solvation free energies (and related data) of neutral solutes [133], and therefore its compatibility with a particular E_{SHE} is unclear.

2. Nonaqueous Systems

In nonaqueous solution, there is no primary reference electrode equivalent to the aqueous SHE or SCE. Nonaqueous silver electrodes using silver nitrate or perchlorate are reliable reference electrodes for nonaqueous solutions; however, details on the actual Ag^+ concentration or salt anion in the Ag^+/Ag are often not reported, making it difficult to directly compare potentials obtained from different studies [54]. Although aqueous reference electrodes are often used for nonaqueous systems, the liquid junction potential between the aqueous and nonaqueous solutions can affect the measurements. For these reasons, the IUPAC Commission on Electrochemistry has recommended

TABLE 6.2
Examples of Commonly Used Solvent Models and the Levels of Theory at Which They Are Applied

Solvent Model	$\Delta G_s^*(H^+)$ (kJ mol ⁻¹)	Level of Theory	E_{SHE} (V)
(C)-PCM-UAHF [149]	-1093.7	HF/6-31G(d) for neutrals and HF/6-31+G(d) for ions	4.47
(C)-PCM-UAKS	-1093.7 ^a	B3LYP or PBE0/6-31+G(d)	4.47
SM6 [130]	-1105.8	MPW25/MIDI!6D or 6-31G(d) or 6-31+G(d) B3LYP/6-31+G(d,p) B3PW91/6-31+G(d,p) and any DFT method that can deliver a reasonably accurate electronic density for the solute of interest	4.34
SMD [127]	-1112.5	Any electronic structure model delivering a reasonable continuous density distribution	4.28
SM8 [129] and SM8AD [128]	-1112.5	HF theory and many local and hybrid density functionals with basis sets of up to minimally augmented polarized valence double-zeta quality	4.28
COSMO-RS [133]	—	BP/TZP	—

The value of the solvation free energy of the proton upon which the model is based and corresponding aqueous E_{SHE} values are also shown.

^a Assumed value.

that the ferrocenium/ferrocene (Fc⁺/Fc) couple be used as an internal reference for reporting electrode potentials in nonaqueous solutions [150], and knowledge of its absolute potential is therefore essential for calculations to be referenced to this electrode.

The absolute potential of the Fc⁺/Fc couple in a nonaqueous solvent can be quite simply obtained from E_{SHE} and the conversion constant between aqueous SHE and (Fc⁺/Fc) in a nonaqueous solvent. Pavlishchuk and Addison determined the conversion constants between various reference electrodes, including the Fc⁺/Fc couple in acetonitrile and aqueous SCE (and SHE) [54]. Thus, using E_{SHE} values of 4.28 and 4.42 V in conjunction with the conversion constant of 0.624 V leads to Fc⁺/Fc potentials of 4.90 and 5.04 V, respectively. More recent calculations using the SMD and COSMO-RS solvent models (in conjunction with gas-phase free energies calculated at G3(MP2)-RAD-Full-TZ and Fermi–Dirac statistics for the electron) provided estimates of 4.96 and 4.99 V for the Fc⁺/Fc potential in acetonitrile, respectively [151]. These values are generally in good agreement with the two “experimental” values of the Fc⁺/Fc potential (within a 100 mV). The choice of Fc⁺/Fc potential for continuum-solvent-based predictions is less obvious, and one could instead adopt an approach analogous to cycle B in Figure 6.2 where both half-cells are treated using the same continuum solvent model.

Related to this point, the reader should note that not all solvent models have been designed to predict solvation free energies in nonaqueous solvents. Examples of models that have been designed to treat nonaqueous solutions are the SMD [127] and the COSMO-RS models [132,133]. The PCM-UAKS and PCM-UAHF models were designed specifically for predicting aqueous free energies of solvation [149], although there have been attempts [152] to extend these models to nonaqueous solvents through the manipulation of other parameters within the solvent model such as the scaling factor (α) that relates to the solvent-inaccessible cavity.

C. STANDARD STATES

When calculating solution-phase reaction energies using a thermodynamic cycle that combines quantities obtained from different sources and/or calculations, it is important to pay attention to the standard state of these quantities. The literature on calculating solvation free energies by quantum

mechanics usually uses a solute standard-state concentration of 1 mol L⁻¹, whereas 1 molal is more common in some other subfields of chemical thermodynamics. The approximation of molality by molarity is reasonable for aqueous solutions since the density of water is approximately 1 kg L⁻¹ for quite a large range of temperatures. This is not necessarily true for solutions involving organic solvents since the density of these solvents is typically much lower.

As noted earlier, the quantity yielded directly by continuum solvation models without a concentration term is the Gibbs free energy change associated with the transfer of a particle in the gas phase to the solvent, where the molarity of the solute is the same in both phases. On the other hand, gas-phase thermodynamic quantities are conventionally calculated using a standard state of 1 atm. The conversion between free energies of solvation in the two conventions is straightforward when we recall the standard states are actually ideal gases and ideal solutions. Thus, the standard-state quantities correspond to measurements at infinite dilution followed by extrapolation to unit activity as if the activity coefficient were unity (ideal behavior). Therefore,

$$\Delta G_S^\circ = \Delta G_S^* + \Delta G_{\text{conc}}^\circ \quad (6.30)$$

where

$$\Delta G_{\text{conc}}^\circ = RT \ln \left(\frac{RT}{P^\circ} \right) \quad (6.30a)$$

where

R is the gas constant

P° is the standard-state pressure

At 298 K, we get $\Delta G_{\text{conc}}^\circ = 7.96$ kJ/mol for $P^\circ = 1$ bar and $\Delta G_{\text{conc}}^\circ = 7.93$ kJ/mol for $P^\circ = 1$ atm.

A separate issue relating to standard states is that experimental measurements are not usually made at either an activity of one or a molarity of one. For example, they may be made in systems buffered to keep particular reactant and/or product concentrations at some convenient concentration. For example, reductive chlorination potentials are nearly always measured with the chloride ion concentration at about 10⁻³ M—these are conditional potentials, but they are not standard or formal potentials; however, they can be converted to standard concentrations. Similarly, to use thermodynamic data in applications, one must convert from tabulated standard-state quantities to quantities pertaining to real experimental conditions. To facilitate the comparison between standard free energies and those pertaining to nonstandard conditions, we note that the Gibbs free energies of reaction at nonstandard concentrations and those at standard concentrations are related by

$$\Delta G = \Delta G^\circ + RT \ln \left(\frac{Q}{Q^\circ} \right) \quad (6.31)$$

where

Q is the reaction quotient

ΔG and Q are for nonstandard concentrations

ΔG° and Q° are for standard states

At equilibrium, $\Delta G = 0$ and Q becomes the equilibrium constant K , so this yields

$$\Delta G^\circ = -RT \ln \left(\frac{K}{Q^\circ} \right) \quad (6.31a)$$

D. RATES OF ELECTRON TRANSFER

The focus of this chapter is on the prediction of standard reduction potentials, and not on kinetics, but we note here that the sum of two standard half reactions defines the standard *driving force* ΔG° for an electron-transfer reaction between a donor D and an acceptor A. For convenience of notation, we will here write D and A as neutral species and the post-electron-transfer products D^+ and A^- as singly positively and negatively charged species, respectively, but there is no restriction on the initial and final charge states beyond the obvious one that after a single electron-transfer D will be one unit more positively charged and A one unit more negatively charged.

In the Marcus theory, the driving force is a key variable for the prediction of free energies of activation associated with electron-transfer reactions. This free energy of activation can be used in a transition-state theory equation or a diabatic collision theory approach to compute rate constants for electron-transfer reactions. In particular, the Marcus theory [153] takes the free energy of activation to be

$$\Delta G^\ddagger = \frac{(\lambda + \Delta G^\circ)^2}{4\lambda} \quad (6.32)$$

where we have omitted some work terms necessary to bring the reagents together and where λ is the *reorganization energy* associated with the electron-transfer reaction. The reorganization energy may be taken as the sum of two components: an *outer-sphere* and an *inner-sphere* reorganization energy. The former is associated with the change in solvation free energy that occurs when a generalized bulk solvent coordinate equilibrated with the pre-electron-transfer state is confronted *instantaneously* with the post-electron-transfer state. Such changes in solvation free energy may be computed using two-time-scale continuum solvation models [154–156] that permit the fast (optical) component of the solvent reaction field to be equilibrated to the post-electron-transfer state while the slow (bulk) component remains frozen as it was equilibrated to the pre-electron-transfer state. The free energy of solvation of the charge-transfer (CT) state interacting with the nonequilibrium two-time-scale reaction field minus the free energy of solvation of the pre-CT state interacting with its fully equilibrated reaction field defines the outer-sphere reorganization energy. The *inner-sphere* reorganization energy, on the other hand, is associated with changes in the donor and acceptor structures (including possibly their first solvation shells) as they relax following the electron transfer.

From a computational standpoint, these various quantities are readily computed. Thus, for instance, by computing the energy change as D^+ relaxes from the geometry of D to that of D^+ (which in some instances may involve including the first solvation shell of D/D^+), one may compute the contribution of the donor molecule to the inner-sphere reorganization energy. Since kinetics is a digression from our main subject, we will not develop this topic further, but we emphasize that the computational techniques outlined here to compute electron-transfer driving forces, combined with approaches to compute reorganization energies, offer a practical avenue to addressing electron-transfer rate questions.

IV. EXAMPLES

This section contains examples of calculations of reduction potential. All calculations were performed using Gaussian 09 [157] or MOLPRO 2009 [158].

A. AQUEOUS STANDARD ONE-ELECTRON REDUCTION POTENTIALS OF NITROXIDES AND QUINONES

In this example, we calculate the standard potentials of the aqueous one-electron reduction half reactions shown in [Figure 6.4](#).

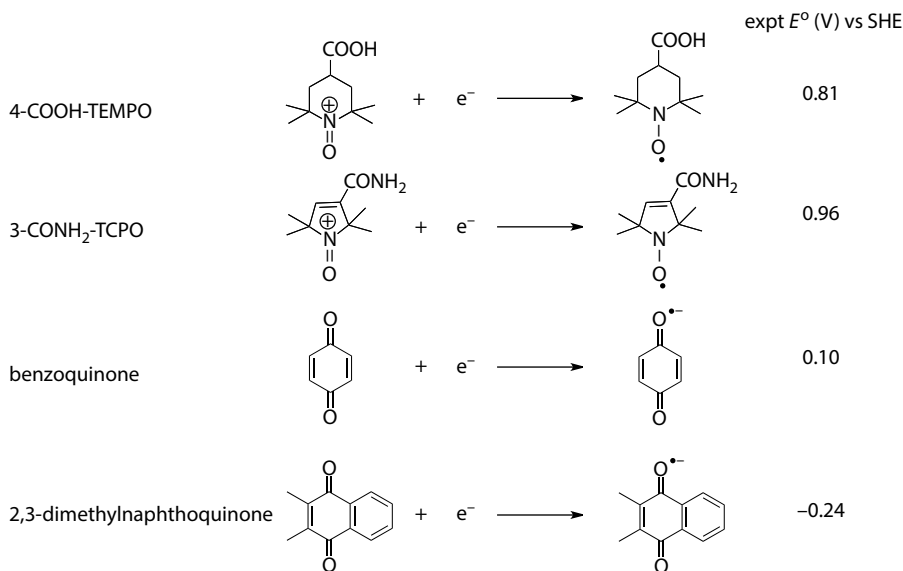


FIGURE 6.4 Species studied with their experimental reduction potentials (see Table 6.3 for details).

The relevant computational data are shown in Table 6.3. The gas-phase Gibbs free energies were computed at the G3(MP2)-RAD(+) level of theory, which is a modification of the G3(MP2)-RAD [71] method. The (+) signifies that calculations originally defined to involve the 6-31G(d) basis set have been carried with the 6-31+G(d) basis set so as to allow for an improved description of anionic species. The aqueous-phase Gibbs free energy of reaction, $\Delta G_{\text{soln}}^\circ$, is calculated using cycle A in Figure 6.2:

$$\Delta G_{\text{soln}}^\circ = G_{\text{gas}}^\circ(\text{Red}) - G_{\text{gas}}^\circ(\text{Ox}) - G_{\text{gas}}^\circ(e) + \Delta G_{\text{S}}^\circ(\text{Red}) - \Delta G_{\text{S}}^\circ(\text{Ox}) \quad (6.33)$$

By substituting the appropriate values into this expression, one obtains the $\Delta G_{\text{soln}}^\circ$ in Table 6.3 and the corresponding standard reduction potentials. The values of 4.47 and 4.28 V for E_{SHE}° were used in conjunction with calculations employing the CPCM-UAHF and SMD solvent models as outlined in Table 6.2.

The table shows that while the approach performs reasonably well for nitroxides, its performance is much less satisfactory for the quinones where the magnitude of the errors is 380 mV or larger for both solvent models. This example illustrates the difficulty associated with the *direct* calculation of absolute reduction potentials where performance depends heavily on the accuracies of absolute solvation free energies of the reactants and products. In particular, all half reactions generate or consume a charged species, and because the uncertainty in the solvation free energies associated of these species are significantly higher, this directly impacts the accuracy of absolute potentials. The present example also illustrates that the good performance of directly calculated reduction potentials by a given method for a particular class of compounds does not necessarily extend to other types of compounds. An interesting observation for the four cases in Table 6.3 is that in every instance, the reduced product would be expected to be a much stronger hydrogen bond acceptor than the oxidized precursor. Thus, first-solvent shell water molecules are very important.

An alternative approach is to calculate *relative* reduction potentials, which can be more accurate by systematic error cancellation. For example, the data in Table 6.3 reveal that calculations based on the CPCM-UAHF model underestimate the standard potentials for quinones by about 600 mV. Such a systematic error will largely cancel out for the reaction shown in Figure 6.5.

The potential associated with this reaction is readily obtained from the data in Table 6.2 as the reduction potential of 2,3-dimethylnaphthoquinone less that of benzoquinone. Using the

TABLE 6.3**Computational Data for the Calculation of Standard Reduction Potentials at 298 K and Relative to SHE^a**

	4-COOH-TEMPO ^g		3-CONH ₂ -TCPO ^g		Benzoquinone		2,3-Dimethylnaphthoquinone	
	Ox	Red	Ox	Red	Ox	Red	Ox	Red
H_0 (kJ mol ⁻¹)	-1,761,669.5	-1,762,348.8	-1,603,319.8	-1,604,000.7	-1,000,069.2	-1,000,250.1	-1,608,881.0	-1,609,042.0
ΔG_{therm} (kJ mol ⁻¹)	-108.5	-110.2	-105.6	-107.6	-78.5	-79.1	-102.5	-101.0
G_{gas}° (kJ mol ⁻¹) ^b	-1,761,778.0	-1,762,459.0	-1,603,425.4	-1,604,108.3	-1,000,147.8	-1,000,329.2	-1,608,983.5	-1,609,143.0
$\Delta G_{\text{S}}^{\circ}$ (UAHF; kJ mol ⁻¹) ^c	-233.2	-42.2	-212.3	-39.9	-28.1	-243.3	-13.5	-209.9
$\Delta G_{\text{S}}^{\circ}$ (SMD; kJ mol ⁻¹) ^c	-242.6	-44.7	-241.9	-52.5	-24.9	-233.0	-19.7	-215.6
$\Delta G_{\text{soln}}^{\circ}$ (UAHF; kJ mol ⁻¹) ^d		-486.3		-506.9		-393.1		-352.2
$\Delta G_{\text{soln}}^{\circ}$ (SMD; kJ mol ⁻¹) ^d		-479.5		-489.9		-386.0		-351.8
E° (UAHF) rel. SHE ^e (V)		0.57 (-0.24)		0.78 (-0.18)		-0.40 (-0.50)		-0.82 (-0.58)
E° (SMD) rel. SHE ^f (V)		0.69 (-0.12)		0.80 (-0.16)		-0.28 (-0.38)		-0.63 (-0.39)
E° (expt)		0.81 [159]		0.96 [159]		0.10 [160]		-0.24 [160]

Signed errors are shown in parentheses.

^a The gas-phase energies were computed at the G3(MP2)-RAD(+) level. Solvation calculations using the CPCM-UAHF and SMD models were performed by the HF/6-31+G(d) and B3LYP/6-31+G(d) methods on the respective solution-phase optimized geometries. CPCM-UAHF solvation free energies were performed at the ROHF/6-31+G(d) level on UHF/6-31+G(d) solution optimized geometries for open-shell species.

^b $G_{\text{gas}}^{\circ} = H_0 + \Delta G_{\text{therm}}$.

^c Solvation free energies printed in Gaussian 09 correspond to $\Delta G_{\text{S}}^{\circ}$ and Equation 6.30 is used to obtain $\Delta G_{\text{S}}^{\circ}$.

^d $\Delta G_{\text{soln}}^{\circ}$ calculated from Equation 6.32.

^e $E_{\text{SHE}} = 4.47$ V.

^f $E_{\text{SHE}} = 4.28$ V.

^g 4-COOH-TEMPO = 2,2,6,6-tetramethylpiperidinoxyl; 3-CONH₂-TCPO = 2,2,5,5-tetramethyl-3-carbamido-3-pyrroline-1-oxyl.



FIGURE 6.5 An isodesmic CT reaction.

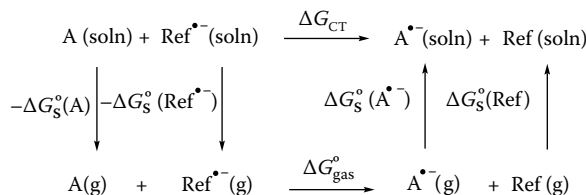


FIGURE 6.6 Thermodynamic cycle for a CT reaction.

CPCM-UAHF model, this CT potential is -0.42 V. Thus, by using benzoquinone as a reference molecule for which the experimental standard potential is known (0.10 V), one can estimate the standard potential of 2,3-dimethylnaphthoquinone by adding the CT potential to $E^{\circ}(\text{benzoquinone})$ to give $E^{\circ}(2,3\text{-dimethylnaphthoquinone}) = -0.32$ V. This approach brings the error down from 580 to 80 mV. More generally, for the CT reaction between A and a reference molecule (Ref) with known E° , the standard potential $E^{\circ}(\text{A}/\text{A}^{\bullet-})$ may be obtained from the thermodynamic cycle in Figure 6.6 and Equation 6.34a:

$$\Delta G_{\text{CT}} = \Delta G_{\text{gas}}^{\circ} + \Delta G_{\text{S}}^{\circ}(\text{A}^{\bullet-}) + \Delta G_{\text{S}}^{\circ}(\text{Ref}) - \Delta G_{\text{S}}^{\circ}(\text{A}) - \Delta G_{\text{S}}^{\circ}(\text{Ref}^{\bullet-}) \quad (6.34)$$

$$E^{\circ}(\text{A}/\text{A}^{\bullet-}) = \frac{\Delta G_{\text{CT}}}{96.5 \text{ C mol}^{-1}} + E_{\text{expt}}^{\circ}(\text{Ref}/\text{Ref}^{\bullet-}) \quad (6.34a)$$

An added advantage of this approach is that E_{SHE}° is no longer needed, thereby eliminating a source of uncertainty. However, since the method relies on systematic error cancellation, it is expected to work best when the reference molecule is structurally similar to A. The major limitation of this approach is that a structurally similar reference with accurately known E° may not always be available.

B. CHEMICALLY IRREVERSIBLE PROCESSES—REDUCTIVE DECHLORINATION

Next, we show how the reduction potentials corresponding to the dissociative electron-transfer reactions of some alkyl halides in aqueous and nonaqueous solutions (Figure 6.7) are calculated. The relevant computational data and results are presented in Tables 6.4 and 6.5, respectively.

Since the potentials of reactions 1, 3, and 4 are measured in DMF and are referenced to the aqueous SCE, a 0.172 V [53] correction for a liquid junction potential was applied to the calculations. Accordingly, using the reductive cleavage of carbon tetrachloride (reaction 3) as example, its reduction potential was calculated as follows:

$$\begin{aligned}
 \Delta G_{\text{soln}} &= -361.4 \text{ kJ mol}^{-1} \\
 E^{\circ} &= \frac{-\Delta G_{\text{soln}}}{96.5} - E_{\text{SHE}}^{\circ} - E^{\circ}(\text{SCE}/\text{SHE}) - E_j \\
 &= 3.75 - 4.28 - 0.241 + 0.172 = -0.60 \text{ V}
 \end{aligned} \quad (6.35)$$

where the calculations are referenced to the aqueous SCE and $E^{\circ}(\text{SCE}/\text{SHE})$ is its potential relative to aqueous SHE (0.241 V) [42].

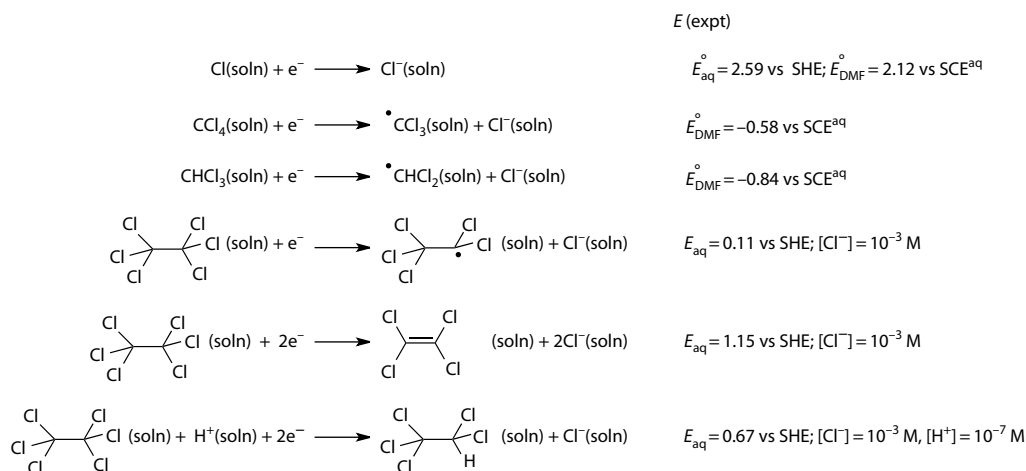


FIGURE 6.7 Species studied with their experimental reduction potentials in V (see Table 6.5 for details).

TABLE 6.4
Calculated Gas-Phase Gibbs Free Energies and Solvation Free Energies at 298 K^a

	Cl^\bullet	$\text{Cl}^-/\text{Cl}^- \cdot \text{H}_2\text{O}$	CCl_4	CCl_3^\bullet	CHCl_3	CHCl_2^\bullet
$G_{\text{gas}}^\circ (\text{kJ mol}^{-1})^{\text{a}}$	-1,206,953.9 ^c	-1,207,306.1/-1,407,825.0	-4,928,225.9	-3,721,026.3	-3,722,725.7	-2,515,500.8
$\Delta G_{\text{S}}^\circ (\text{SMD}) \text{H}_2\text{O}^{\text{b}}$	8.4	-/-260.3	—	—	—	—
$\Delta G_{\text{S}}^\circ (\text{SMD}) \text{DMF}^{\text{b}}$	1.8	-264.8/—	-4.2	2.1	-12.9	-0.8
	C_2Cl_6	$\text{C}_2\text{Cl}_5^\bullet$	C_2HCl_5	C_2Cl_4	H^+	H_2O
$G_{\text{gas}}^\circ (\text{kJ mol}^{-1})^{\text{a}}$	-7,442,299.2	-6,235,086.3	-6,236,794.9	-5,028,088.6	-26.3	-200,483.0
$\Delta G_{\text{S}}^\circ (\text{SMD}) \text{H}_2\text{O}^{\text{b}}$	13.2	13.9	3.0	15.7	-1,104.6	—

^a Computed at the G3(MP2)-RAD(+) level of theory.

^b Calculations (in kJ mol^{-1}) performed by the B3LYP/6-31+G(d) method on solution-phase optimized geometries.

^c Includes spin-orbit correction (-1.34 millihartrees).

As mentioned in Section III.B, first-solvent shell interactions are likely to be very important for species with regions of concentrated charge such that a continuum model is likely to be inadequate. The reader should therefore note that the SMD, SM6, and SM8 solvent models are to be used as mixed discrete-continuum models in such cases; in particular, they have been parameterized to reproduce the experimental aqueous solvation free energy of the $\text{Cl}^- \cdot \text{H}_2\text{O}$ cluster and $(\text{H}_2\text{O})_2$ dimer, not the solvation free energy of bare Cl^- or H_2O [33,127,129,130]. As such, for the aqueous reactions that involve a bare chloride ion, that is, reactions 2 and 5 to 7, the calculations were carried out with the addition of a water of hydration, as shown in Table 6.5. Using the last reaction as example, the calculated $\Delta G_{\text{soln}}^\circ$ was obtained as follows:

$$\Delta G_{\text{soln}}^\circ = \Delta G_{\text{gas}}^\circ + \Delta \Delta G_{\text{S}}^\circ = -961.5 \text{ kJ mol}^{-1} \quad (6.36)$$

where

$$\begin{aligned} \Delta \Delta G_{\text{S}}^\circ &= \Delta G_{\text{S}}^\circ (\text{Cl}^- \cdot \text{H}_2\text{O}) + \Delta G_{\text{S}}^\circ (\text{C}_2\text{HCl}_5) - \Delta G_{\text{S}}^\circ (\text{H}^+) - \Delta G_{\text{S}}^\circ (\text{C}_2\text{Cl}_6) - \Delta G_{\text{S}}^\circ (\text{H}_2\text{O}) \\ &= 842.6 \text{ kJ mol}^{-1} \end{aligned} \quad (6.37)$$

TABLE 6.5
Calculated Reduction Potentials and Experimental Values^a

		<i>E/V (calc)</i>	<i>E/V (expt)</i>
1	$\text{Cl}^*(\text{dmf}) + e^- \rightarrow \text{Cl}^-(\text{dmf})$	2.03	2.12 [161]
2	$\text{Cl}^*(\text{aq}) + \text{H}_2\text{O}(\text{l}) + e^- \rightarrow [\text{Cl}(\text{H}_2\text{O})]^- (\text{aq})$	2.40 ^c	2.59 [161]
3	$\text{CCl}_4(\text{dmf}) + e^- \rightarrow \text{CCl}_3^*(\text{dmf}) + \text{Cl}^-(\text{dmf})$	-0.60	-0.58 [162]
4	$\text{CHCl}_3(\text{dmf}) + e^- \rightarrow \text{CHCl}_2^*(\text{dmf}) + \text{Cl}^-(\text{dmf})$	-0.93	-0.84 [162]
5	$\text{C}_2\text{Cl}_6(\text{aq}) + \text{H}_2\text{O}(\text{l}) + e^- (\text{g}) \rightarrow \text{C}_2\text{Cl}_5^*(\text{aq}) + [\text{Cl}(\text{H}_2\text{O})]^- (\text{aq})$	-0.20 ^{b,c}	0.11 ^b [1]
6	$\text{C}_2\text{Cl}_6(\text{aq}) + 2\text{H}_2\text{O}(\text{l}) + 2e^- (\text{g}) \rightarrow \text{C}_2\text{Cl}_4(\text{aq}) + 2[\text{Cl}(\text{H}_2\text{O})]^- (\text{aq})$	0.91 ^{b,c}	1.15 ^b [1]
7	$\text{C}_2\text{Cl}_6(\text{aq}) + \text{H}_2\text{O}(\text{l}) + \text{H}^+ (\text{aq}) + 2e^- (\text{g}) \rightarrow \text{C}_2\text{HCl}_5(\text{aq}) + [\text{Cl}(\text{H}_2\text{O})]^- (\text{aq})$	0.58 ^{b,c}	0.67 ^b [1]

^a Reactions in DMF and aqueous solution are referenced to SCE(aq) and SHE(aq), respectively.

^b These potentials correspond to the experimental conditions $[\text{Cl}^-] = 10^{-3} \text{ mol L}^{-1}$ and $\text{pH} = 7$.

^c Calculations that include an explicit water of hydration. The experimental solvation free energy of the water (-8.6 kJ mol^{-1}) that corresponds to a standard state of $[\text{H}_2\text{O}] = 55 \text{ mol L}^{-1}$ (i.e., pure water) and 1 atm in the liquid and gas phase was used in these calculations.

Note that in these calculations, we have used the experimental value for the solvation free energy for water (-8.6 kJ mol^{-1}) [163] under the conventional standard state for pure liquids, that is, mole fraction of 1 in the liquid phase and 1 atm in the gas phase. In these reactions, the experimental potentials for the reductive cleavage of hexachloroethane were referenced to SHE, and therefore no correction for E_j was applied. However, the potentials corresponded to nonstandard conditions of $[\text{Cl}^-] = 10^{-3} \text{ mol L}^{-1}$ and $\text{pH} 7$, and a correction using Equation 6.31 was applied to arrive at the values in Table 6.5:

$$\begin{aligned} \Delta G_{\text{soln}} &= \Delta G_{\text{soln}}^\circ + RT \ln \left(\frac{([1 \text{ M C}_2\text{HCl}_5][10^{-3} \text{ M Cl}^-]/[1 \text{ M C}_2\text{Cl}_6][10^{-7} \text{ M H}^+])}{([1 \text{ M C}_2\text{HCl}_5][1 \text{ M Cl}^-]/[1 \text{ M C}_2\text{Cl}_6][1 \text{ M H}^+])} \right) \\ &= \Delta G_{\text{soln}}^\circ + RT \ln(10^4) = -938.7 \text{ kJ mol}^{-1} \end{aligned} \quad (6.38)$$

Accordingly, the potential for this two-electron reduction is

$$E = -\frac{-938.7}{2 \times 96.5} - 4.28 = 0.58 \text{ V} \quad (6.39)$$

C. CONSTRUCTING A POURBAIX DIAGRAM FOR THE TWO-ELECTRON REDUCTION OF *o*-CHLORANIL

Consider the two-electron reduction of *o*-chloranil (OCA) in aqueous solution [164]. Depending on the pH of the solution, the reduction process can be represented in one of the following ways as shown in Figure 6.8.

The corresponding standard reduction potentials are denoted $E^\circ(\text{OCA}/\text{OCA}^{2-})$, $E^\circ(\text{OCA}, \text{H}^+/\text{OCAH}^-)$, and $E^\circ(\text{OCA}, 2\text{H}^+/\text{OCAH}_2)$, and these are related to each other as follows:

$$E^\circ(\text{OCA}/\text{OCA}^{2-}) = E^\circ(\text{OCA}, \text{H}^+/\text{OCAH}^-) + \frac{RT}{2F} \ln K_2 \quad (6.40)$$

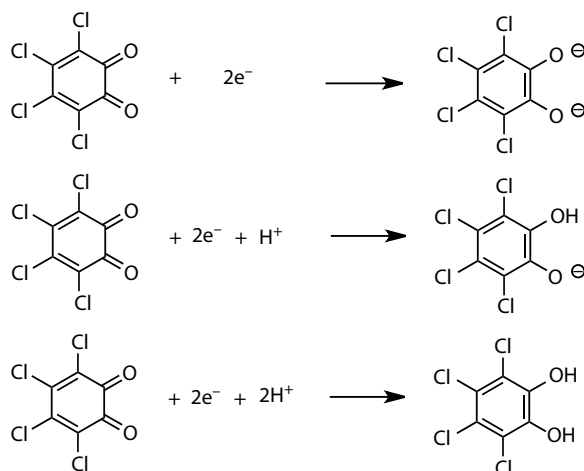


FIGURE 6.8 The microspecies present in the two-electron reduction of OCA in aqueous solution.

$$E^\circ(\text{OCA}/\text{OCA}^{2-}) = E^\circ(\text{OCA}, 2\text{H}^+/\text{OCAH}_2) + \frac{RT}{2F} \ln K_1 K_2 \quad (6.41)$$

where K_1 and K_2 are the first and second acid dissociation constants of OCAH_2 . From Equation 6.11, the potential for the $E(\text{OCA}, 2\text{H}^+/\text{OCAH}_2)$ is

$$E = E^\circ(\text{OCA}, 2\text{H}^+/\text{OCAH}_2) + \frac{RT}{2F} \ln \frac{[\text{OCA}^{2-}][\text{H}^+]^2}{[\text{OCAH}_2]} \quad (6.42)$$

Equation 6.42 can alternatively be expressed in terms of the acid dissociation constants (K_1 and K_2) of the conjugate acid of the reduced product (H_2A):

$$E = E^\circ(\text{OCA}, 2\text{H}^+/\text{OCA}^{2-}) + \frac{RT}{2F} \ln (K_1 K_2 + K_1 [\text{H}^+] + [\text{H}^+]^2) + \frac{RT}{2F} \ln \frac{S_{\text{Ox}}}{S_{\text{Red}}} \quad (6.43)$$

$$S_{\text{Ox}} = [\text{OCA}] \quad (6.43a)$$

$$S_{\text{Red}} = [\text{OCA}^{2-}] + [\text{OCAH}^-] + [\text{OCAH}_2] \quad (6.43b)$$

Using techniques such as cyclic voltammetry, one can measure a half-wave potential ($E_{1/2}$) where the concentrations of the reductant are approximately equal to the oxidant, that is, $S_{\text{Ox}} = S_{\text{Red}}$, and Equation 6.43 becomes

$$E_{1/2} = E^\circ(\text{OCA}, 2\text{H}^+/\text{OCA}^{2-}) + \frac{RT}{2F} \ln (K_1 K_2 + K_1 [\text{H}^+] + [\text{H}^+]^2) \quad (6.44)$$

TABLE 6.6
Calculated^a Reduction Potentials in V and p*K*_a Values

$E^\circ(\text{OCA}, 2\text{H}^+/\text{OCAH}_2)$	0.83 (0.79) [164]
$E^\circ(\text{OCA}, \text{H}^+/\text{OCAH}^-)$	0.63 (0.67) [164]
$E^\circ(\text{OCA}/\text{OCA}^{2-})$	0.41 ^b
p <i>K</i> ₁	(5) [164]
p <i>K</i> ₂	9.2 ^c

Experimental values, where available, are shown in parentheses.

^a Calculations are based on the G3(MP2)-RAD(+) gas-phase energies with SMD solvation energies obtained at the B3LYP/6-31+G(d) level and E_{SHE} of 4.28 V.

^b Calculated from Equation 6.40 using the data in this table.

^c Calculated using a proton-exchange method [34,35] using orthoquinone (expt p*K*_a = 13.4) [165] as the reference.

From the calculated reduction potentials in Equations 6.40 and 6.41 as well as the acid dissociation constants (K_1 and K_2) of the diprotic acid, OCAH_2 , a chemical speciation plot denoting the dominant microspecies in a particular pH range can be obtained. The data needed for such a plot are shown in Table 6.6.

From Equation 6.43, three distinct linear pH ranges can readily be identified. In the range where $\text{pH} < \text{p}K_1$, $[\text{H}^+] \gg K_1 \gg K_2$, the molecule OCAH_2 is the predominant form of the reduced product, and the midpoint potential has a pH dependence based on Equation 6.44:

$$E_{1/2} = E^\circ(\text{OCA}, 2\text{H}^+/\text{OCAH}_2) + \frac{RT}{2F} \ln[\text{H}^+]^2 \quad (6.45)$$

In the other two linear segments at $\text{p}K_1 < \text{pH} < \text{p}K_2$ and $\text{pH} > \text{p}K_2$, the reduced product exists predominantly as OCAH^- and OCA^{2-} , respectively, and the corresponding half-wave potentials have pH dependence following equations:

$$E_{1/2} = E^\circ(\text{OCA}, 2\text{H}^+/\text{OCAH}_2) + \frac{RT}{2F} \ln(K_1[\text{H}^+]) \quad (6.46)$$

$$E_{1/2} = E^\circ(\text{OCA}, 2\text{H}^+/\text{OCAH}_2) + \frac{RT}{2F} \ln(K_1K_2) \quad (6.47)$$

Extrapolation of the three linear segments (with theoretical slopes $-2.303mRT/2F$, where m is the number of protons involved in the reaction) to pH 0 yields the formal potential $E^\circ(\text{OCA}, 2\text{H}^+/\text{OCAH}_2)$, $E^\circ(\text{OCA}, \text{H}^+/\text{OCAH}^-)$, and $E^\circ(\text{OCA}/\text{OCA}^{2-})$, respectively. Collectively, this information can be used to construct a E versus pH (Pourbaix diagram) as shown in Figure 6.9. The vertical lines correspond to the p*K*_as of the diprotic OCAH_2 acid.

The reader should note that the formal potential E° is pH invariant since the condition $[\text{H}^+] = 1 \text{ mol L}^{-1}$ applies. However, half-wave potentials are strongly pH dependent, and these are quite often reported instead of standard or formal reduction potentials. Thus, in comparing with experiment, it is also important to examine the details of the experimental measurement to ascertain whether the calculation corresponds to the same quantity as the one reported.

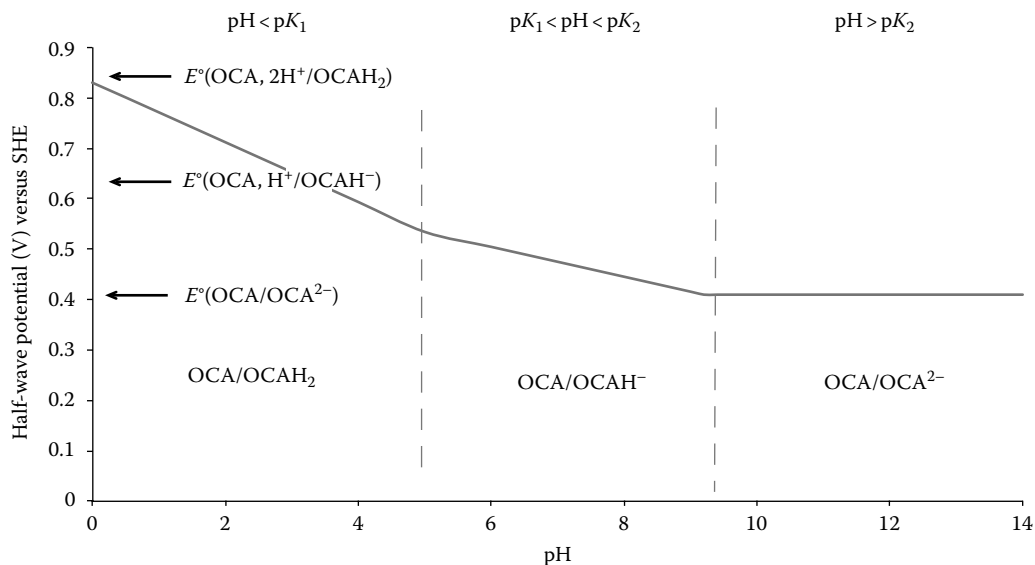


FIGURE 6.9 An E versus pH diagram (Pourbaix diagram) for OCA. The vertical dotted lines correspond to the $\text{p}K_{\text{a}}$ s of OCAH_2 and indicate the pH regions in which various stable species predominate.

V. CONCLUDING REMARKS

We have presented an introductory guide to carrying out QM continuum solvent prediction of solution-phase reduction potentials. We stress that reduction potentials are equilibrium thermochemical parameters. We discussed issues pertaining to thermochemical conventions for the electron, the choice of standard electrode, and the advantages and limitations of methods based on thermodynamic cycles for calculating reduction potentials. Just as in experimental work, a key consideration for predicting chemically accurate reduction potentials is the difficulty of obtaining accurate estimates of the solvation free energies of ionic species. Careful work often involves including (or expanding) a first solvation shell, particularly in solvents donating or accepting strong hydrogen bonds. Relative reduction potential calculations can partly remedy this problem by exploiting systematic error cancellation in the solvation calculations.

ACKNOWLEDGMENTS

We gratefully acknowledge support from the Australian Research Council under their Centres of Excellence program and the generous allocation of computing time on the National Facility of the National Computational Infrastructure. MLC also acknowledges an ARC Future Fellowship. This work was supported in part by the U.S. Army Research Lab under Grant No. W911NF09-1-0377 and the U.S. National Science Foundation under Grant No. CHE09-56776.

REFERENCES

1. Patterson, E. V.; Cramer, C. J.; Truhlar, D. G. *J. Am. Chem. Soc.* **2001**, *123*, 2025–2031.
2. Lewis, A.; Bumpus, J. A.; Truhlar, D. G.; Cramer, C. J. *J. Chem. Ed.* **2004**, *81*, 596–604; Erratum: **2007**, *84*, 934.
3. Vogel, T. M.; Criddle, C. S.; McCarty, P. L. *Environ. Sci. Technol.* **1987**, *21*, 722–736.
4. Totten, L. A.; Roberts, A. L. *Crit. Rev. Environ. Sci. Technol.* **2001**, *31*, 175–221.
5. Olivas, Y.; Dolfing, J.; Smith, G. B. *Environ. Toxicol. Chem.* **2002**, *21*, 493–499.
6. van Pee, K. H.; Unversucht, S. *Chemosphere* **2002**, *52*, 299.
7. Bylaska, E. J.; Dupuis, M.; Tratynek, P. G. *J. Phys. Chem. A* **2005**, *109*, 5905–5916.

8. Cwierty, D. M.; Arnold, W. A.; Kohn, T.; Rodenburg, L. A.; Roberts, A. L. *Environ. Sci. Technol.* **2010**, *44*, 7928–7936.
9. Krishna, M. C.; Grahame, D. A.; Samuni, A.; Mitchell, J. B.; Russo, A. *Proc. Natl. Acad. Sci. USA* **1992**, *89*, 5537–5541.
10. Mitchell, J. B.; Samuni, A.; Krishna, M. C.; DeGraff, W.; Ahn, M. S.; Samuni, U.; Russo, A. *Biochemistry* **1990**, *29*, 2802–2807.
11. Samuni, A.; Krishna, M. C.; Mitchell, J. B.; Collins, C. R.; Russo, A. *Free Radic. Res. Commun.* **1990**, *9*, 241–249.
12. Kinoshita, Y.; Yamada, K.-I.; Yamasaki, T.; Mito, F.; Yamoto, M.; Kosem, N.; Deguchi, H.; Shirahama, C.; Ito, Y.; Kitagawa, K.; Okukado, N.; Sakai, K.; Utsumi, H. *Free Radic. Biol. Med.* **2010**, *49*, 1703–1709.
13. Blinco, J. P.; Hodgson, J. L.; Morrow, B. J.; Walker, J. R.; Will, G. D.; Coote, M. L.; Bottle, S. E. *J. Org. Chem.* **2008**, *73*, 6763–6771.
14. Hodgson, J. L.; Namazian, M.; Bottle, S. E.; Coote, M. L. *J. Phys. Chem. A* **2007**, *111*, 13595–13605.
15. Winget, P.; Cramer, C. J.; Truhlar, D. G. *Theor. Chem. Acc.* **2004**, *112*, 217–227.
16. Philips, K. L.; Sandler, S. I.; Chiu, P. C. *J. Comput. Chem.* **2010**, *32*, 226–239.
17. Speelman, A. L.; Gilmore, J. G. *J. Phys. Chem. A* **2008**, *112*, 5684–5690.
18. Winget, P.; Weber, E. J.; Cramer, C. J.; Truhlar, D. G. *Phys. Chem. Chem. Phys.* **2000**, *2*, 1231–1239.
19. Hicks, L. D.; Fry, A. J.; Kurzwil, V. C. *Electrochim. Acta* **2004**, *50*, 1039–1047.
20. Alston, J. Y.; Fry, A. J. *Electrochim. Acta* **2004**, *49*, 455–459.
21. Wolfe, J. J.; Wright, J. D.; Reynolds, C. A.; Saunders, A. C. G. *Anti-Cancer Drug Des.* **1994**, *9*, 85–102.
22. Bottoni, A.; Cosimelli, B.; Scavetta, E.; Spinelli, D.; Spisani, R.; Stenta, M.; Tonelli, D. *Mol. Phys.* **2006**, *104*, 2961–2974.
23. Shamsipur, M.; Sirouejnejad, A.; Hemmateenejad, B.; Abbaspour, A.; Sharghi, H.; Alizadeh, K.; Arshadi, S. *J. Electroanal. Chem.* **2007**, *600*, 345–358.
24. Crespo-Hernandez, C. E.; Close, D. M.; Gorb, L.; Leszczynski, J. *J. Phys. Chem. B* **2007**, *111*, 5386–5395.
25. Cody, J.; Mandal, S.; Yang, L. C.; Fahrni, C. J. *J. Am. Chem. Soc.* **2008**, *130*, 13023–13032.
26. Moens, J.; Jaque, P.; De Proft, F.; Geerlings, P. *J. Phys. Chem. A* **2008**, *112*, 6023–6031.
27. Moens, J.; Geerlings, P.; Roos, G. *Chem. Eur. J.* **2007**, *13*, 8174–8184.
28. Moens, J.; Roos, G.; Jaque, P.; Proft, F. D.; Geerlings, P. *Chem. Eur. J.* **2007**, *13*, 9331–9343.
29. Sattelle, B. M.; Sutcliffe, M. J. *J. Phys. Chem. A* **2008**, *112*, 13053–13057.
30. Olsson, M. H. M.; Hong, G.; Warshel, A. J. *Am. Chem. Soc.* **2003**, *125*, 5025–5039.
31. Bhattacharyya, S.; Stankovich, M. T.; Truhlar, D. G.; Gao, J. *J. Phys. Chem. A* **2007**, *111*, 5729–5742.
32. Blumberger, J.; Tateyama, Y.; Sprik, M. *Comput. Phys. Commun.* **2005**, *2005*, 256–261.
33. Kelly, C. P.; Cramer, C. J.; Truhlar, D. G. *J. Phys. Chem. A* **2006**, *110*, 2493–2499.
34. Ho, J.; Coote, M. L. *Theor. Chem. Acc.* **2010**, *125*, 3–21.
35. Ho, J.; Coote, M. L. *Comput. Mol. Sci.* **2011**, *1*, 649–660.
36. Lin, C. Y.; Izgorodina, E. I.; Coote, M. L. *Macromolecules* **2010**, *43*, 553–560.
37. Coote, M. L. *Macromol. Theory Simul.* **2009**, *18*, 388–400.
38. Scholz, F. In *Electroanalytical Methods: Guide to Experiments and Applications*; Scholz, F., ed., 2nd edn., Vol. 210; Springer: Berlin, Germany, 2005; p. 20.
39. Lewis, G. N.; Randall, M.; Pitzer, K. S.; Brewer, L. *Thermodynamics*; McGraw-Hill: New York, 1961; p. 353.
40. Berry, R. S.; Ross, S. A. *Physical Chemistry*, 2nd edn.; Oxford University Press: New York, 2000; p. 749.
41. Ramette, R. W. *J. Chem. Ed.* **1987**, *64*, 885.
42. Isse, A. A.; Gennaro, A. *J. Phys. Chem. B* **2010**, *114*, 7894–7899.
43. Bard, A. J.; Faulkner, L. R. *Electrochemical Methods: Fundamentals and Applications*, 2nd edn.; John Wiley & Sons, Inc.: New York, 2001.
44. Quan, M.; Sanchez, D.; Wasylkiw, M. F.; Smith, D. K. *J. Am. Chem. Soc.* **2007**, *129*, 12847–12856.
45. Pourbaix, M. J. N.; Yang, H.-Z.; Zhang, H. M.; Zhang, Z. C. *Corros. Sci.* **1986**, *26*, 873–917.
46. Delahay, P.; Pourbaix, M. J. N.; Van Rysselberghe, P. *J. Chem. Ed.* **1950**, *27*, 683–688.
47. Pourbaix, M. J. N.; Rorive-Bouté, C. M. *Discuss. Faraday Soc.* **1948**, *4*, 139–153.
48. Kato, Y.; Shimizu, Y.; Lin, Y.; Unoura, K.; Utsumi, H.; Ogata, T. *Electrochim. Acta* **1995**, *40*, 2799–2802.
49. Cramer, C. J.; Truhlar, D. G. In *Trends and Perspectives in Modern Computational Science*; Marouli, G.; Simos, T. E., eds.; Brill/SP: Leiden, the Netherlands, 2006; pp. 112–140.
50. Arnold, W.; Winget, P.; Cramer, C. J. *Environ. Sci. Technol.* **2002**, *36*, 3536–3541.
51. O'Malley, T. F. *Phys. Rev.* **1966**, *150*, 14–29.
52. Khare, S. P.; Prakash, S.; Meath, W. J. *Int. J. Mass Spectrom. Ion Process.* **1989**, *88*, 299–308.
53. Diggle, J. W.; Parker, A. J. *Aust. J. Chem.* **1974**, *27*, 1617–1621.
54. Pavlishchuk, V. V.; Addison, A. W. *Inorg. Chim. Acta* **2000**, *298*, 97–102.

55. Alecu, I. M.; Zheng, J.; Zhao, Y.; Truhlar, D. G. *J. Chem. Theory Comput.* **2010**, *6*, 2872–2887.
56. Merrick, J. P.; Moran, D.; Radom, L. *J. Phys. Chem. A* **2007**, *111*, 11683–11700.
57. Scott, A. P.; Radom, L. *J. Phys. Chem.* **1996**, *100*, 16502–16513.
58. Yu, T.; Zheng, J.; Truhlar, D. G. *Phys. Chem. Chem. Phys.* **2012**, *14*, 482–494.
59. Cramer, C. J.; Truhlar, D. G. *J. Am. Chem. Soc.* **1993**, *115*, 5745–5753.
60. Zheng, J.; Yu, T.; Papajak, E.; Alecu, I. M.; Mielke, S. M.; Truhlar, D. G. *Phys. Chem. Chem. Phys.* **2011**, *13*, 10885–10907.
61. Kirkpatrick, S.; Gelatt, Jr., C. D.; Vecchi, M. P. *Science* **1983**, *220*, 671–680.
62. Chang, G.; Guida, W. E.; Still, W. C. *J. Am. Chem. Soc.* **1989**, *111*, 4379–4386.
63. Izgorodina, E. I.; Lin, C. Y.; Coote, M. L. *Phys. Chem. Chem. Phys.* **2007**, *9*, 2507–2516.
64. See, for example, (a) McQuarrie, D.; Simon, J. D. *Physical Chemistry: A Molecular Approach*; University Science Books: Sausalito, CA, 1997. (b) Atkins, P. W. *Physical Chemistry*, 6th edn.; Oxford University Press: Oxford, U.K., 1998.
65. Lin, C. Y.; Izgorodina, E. I.; Coote, M. L. *J. Phys. Chem. A* **2008**, *112*, 1956–1964.
66. Dahlke, E. A.; Truhlar, D. G. *J. Phys. Chem. B* **2006**, *110*, 10595–10601.
67. Raghavachari, K.; Anderson, J. B. *J. Phys. Chem.* **1996**, *100*, 12960–12973.
68. Curtiss, L. A.; Redfern, P. C.; Raghavachari, K. *J. Chem. Phys.* **2007**, *126*, 084108/084101–084112.
69. Curtiss, L. A.; Raghavachari, K.; Redfern, P. C.; Rassolov, V.; Pople, J. A. *J. Chem. Phys.* **1998**, *109*, 7764–7776.
70. Curtiss, L. A.; Redfern, P. C.; Raghavachari, K.; Rassolov, V.; Pople, J. A. *J. Chem. Phys.* **1999**, *110*, 4703–4709.
71. Henry, D. J.; Sullivan, M. B.; Radom, L. *J. Chem. Phys.* **2003**, *118*, 4849–4860.
72. Henry, D. J.; Parkinson, C. J.; Mayer, P. M.; Radom, L. *J. Phys. Chem. A* **2001**, *105*, 6750–6756.
73. Fast, P. L.; Truhlar, D. G. *J. Phys. Chem. A* **2000**, *104*, 6111–6116.
74. Fast, P. L.; Corchado, J. C.; Sánchez, M. L.; Truhlar, D. G. *J. Phys. Chem. A* **1999**, *103*, 5129–5136.
75. Fast, P. L.; Sánchez, M. L.; Corchado, J. C.; Truhlar, D. G. *J. Chem. Phys.* **1999**, *110*, 11679–11681.
76. Fast, P. L.; Sánchez, M. L.; Truhlar, D. G. *Chem. Phys. Lett.* **1999**, *306*, 407–410.
77. Tratz, C. M.; Fast, P. L.; Truhlar, D. G. *PhysChemComm* **1999**, *2*, 70–79.
78. Lynch, B. J.; Truhlar, D. G. *ACS Symp. Ser.* **2007**, *958*, 153–167.
79. Lynch, B. J.; Zhao, Y.; Truhlar, D. G. *J. Phys. Chem. A* **2003**, *107*, 1384–1388.
80. Lynch, B. J.; Truhlar, D. G. *J. Phys. Chem. A* **2003**, *107*, 3898–3906.
81. Curtiss, L. A.; Radfern, P. C.; Rassolov, V.; Kedziora, G.; Pople, J. A. *J. Chem. Phys.* **2001**, *114*, 9287–9295.
82. Curtiss, L. A.; Raghavachari, K.; Redfern, P. C.; Pople, J. A. *J. Chem. Phys.* **2000**, *112*, 1125–1132.
83. DeYonker, N. J.; Williams, T. G.; Imel, A. E.; Cundari, T. R.; Wilson, A. K. *J. Chem. Phys.* **2009**, *131*, 024106/024101–024109.
84. DeYonker, N. J.; Cundari, T. R.; Wilson, A. K. *J. Chem. Phys.* **2006**, *124*, 114104/114101–114117.
85. Montgomery, Jr., J. A.; Frisch, M. J.; Ochterski, J. W.; Petersson, G. A. *J. Chem. Phys.* **1999**, *110*, 2822–2827.
86. Boese, D.; Oren, M.; Atasoylu, O.; Martin, J. M. L.; Kállay, M.; Gauss, J. *J. Chem. Phys.* **2004**, *120*, 4129–4141.
87. Martin, J. M. L.; Parthiban, S. In *Quantum Mechanical Prediction of Thermochemical Data*; Cioslowski, J., ed.; Understanding Chemical Reactivity series, Vol. 22; Kluwer-Academic Publishers: Dordrecht, the Netherlands, 2001; pp. 31–65.
88. Martin, J. M. L.; Oliveira, G. D. *J. Chem. Phys.* **1999**, *111*, 1843–1856.
89. Karton, A.; Martin, J. M. L. *J. Chem. Phys.* **2010**, *133*, 144102/144101–144117.
90. Vreven, T.; Morokuma, K. *J. Comput. Chem.* **2000**, *21*, 1419–1432.
91. Vreven, T.; Morokuma, K. *J. Chem. Phys.* **1999**, *111*, 8799–8803.
92. Izgorodina, E. I.; Brittain, D. R. B.; Hodgson, J. L.; Krenske, E. H.; Lin, C. Y.; Namazian, M.; Coote, M. L. *J. Phys. Chem. A* **2007**, *111*, 10754–10768.
93. Feller, D. *J. Chem. Phys.* **1992**, *96*, 6104–6114.
94. Martin, J. M. L. *Chem. Phys. Lett.* **1996**, *259*, 669–678.
95. Truhlar, D. G. *Chem. Phys. Lett.* **1998**, *294*, 45–48.
96. Schwenke, D. W. *J. Chem. Phys.* **2005**, *122*, 014107/014101–014107.
97. Cramer, C. J.; Truhlar, D. G. *Phys. Chem. Chem. Phys.* **2009**, *11*, 10757–10816.
98. Peverati, R.; Truhlar, D. G. *J. Phys. Chem. Lett.* **2011**, *2*, 2810–2817.
99. Dyall, K. G.; Faegri, K. *Introduction to Relativistic Quantum Chemistry*; Oxford University Press: New York, 2007.
100. Phillips, J. C.; Kleinman, L. *Phys. Rev.* **1959**, *116*, 287–294.
101. Kahn, L. R.; Baybutt, P.; Truhlar, D. G. *J. Chem. Phys.* **1976**, *65*, 3826–3853.

102. Stevens, W. J.; Basch, H.; Krauss, M. *J. Chem. Phys.* **1984**, *81*, 6026–6033.
103. Stoll, H.; Metz, B.; Dolg, M. *J. Comput. Chem.* **2002**, *23*, 767–778.
104. Roy, L. E.; Hay, P. J.; Martin, R. L. *J. Chem. Theory Comput.* **2008**, *4*, 1029–1031.
105. Dolg, M.; Cao, X. *Chem. Rev.* **2012**, *112*, 403–480.
106. Xu, X.; Truhlar, D. G. *J. Chem. Theory Comput.* **2012**, *8*, 80–90.
107. Douglas, M.; Kroll, N. M. *Ann. Phys.* **1974**, *82*, 89–155.
108. Hess, B. A. *Phys. Rev. A* **1986**, *33*, 3742–3748.
109. Nakajima, T.; Hirao, K. *Chem. Rev.* **2012**, *112*, 385–402.
110. van Lenthe, E.; Baerends, E. J.; Snijders, J. G. *J. Chem. Phys.* **1994**, *101*, 9783–9792.
111. Havlas, Z.; Kyvela, M.; Michl, J. In *Computational Methods in Photochemistry*; Kutateladze, A. G., ed.; Taylor & Francis: Boca Raton, FL, 2005; p. 111.
112. Lias, S. G.; Bartmess, J. E.; Mallard, W. G.; Linstrom, P. J., *NIST Chemistry Webbook*; National Institute of Standards and Technology: Gaithersburg, MD, **2012** (<http://webbook.nist.gov>, accessed March 4, 2012).
113. Ervin, K. M. *Chem. Rev.* **2001**, *101*, 391–444.
114. Bartmess, J. E. *J. Phys. Chem.* **1994**, *98*, 6420–6424.
115. Tomasi, J.; Mennucci, B.; Cammi, R. *Chem. Rev.* **2005**, *105*, 2999–3093.
116. Cramer, C. J.; Truhlar, D. G. *Chem. Rev.* **1999**, *99*, 2161–2200.
117. Orozco, M.; Luque, F. J. *Chem. Rev.* **2000**, *100*, 4187–4226.
118. Cramer, C. J.; Truhlar, D. G. *Acc. Chem. Res.* **2008**, *41*, 760–768.
119. Wangsness, R. K. *Electromagnetic Fields*; Wiley: New York, 1979; p. 179.
120. Cancas, M. T.; Mennucci, B.; Tomasi, J. *J. Chem. Phys.* **1997**, *107*, 3032–3041.
121. Cossi, M.; Rega, N.; Scalmani, G.; Barone, V. *J. Comput. Chem.* **2003**, *24*, 669–681.
122. Barone, V.; Cossi, M. *J. Phys. Chem. A* **1998**, *102*, 1995–2001.
123. Cramer, C. J.; Truhlar, D. G. *Acc. Chem. Res.* **2009**, *42*, 493–497.
124. Cramer, C. J.; Truhlar, D. G. *J. Am. Chem. Soc.* **1991**, *113*, 8305–8311.
125. Luque, F. J.; Negre, M. J.; Orozco, M. *J. Phys. Chem.* **1993**, *97*, 4386–4391.
126. Marten, B.; Kim, K.; Cortis, C.; Friesner, R.; Murphy, R. B.; Ringnalda, M. N.; Sitkoff, D.; Honig, B. *J. Phys. Chem.* **1996**, *100*, 11775–11788.
127. Marenich, A. V.; Cramer, C. J.; Truhlar, D. G. *J. Phys. Chem. B* **2009**, *113*, 6378–6396.
128. Marenich, A. V.; Cramer, C. J.; Truhlar, D. G. *J. Chem. Theory Comput.* **2009**, *5*, 2447–2464.
129. Marenich, A. V.; Olson, R. M.; Kelly, C. P.; Cramer, C. J.; Truhlar, D. G. *J. Chem. Theory Comput.* **2007**, *3*, 2011–2033.
130. Kelly, C. P.; Cramer, C. J.; Truhlar, D. G. *J. Chem. Theory Comput.* **2005**, *1*, 1133–1152.
131. Hawkins, G. D.; Zhu, T.; Li, J.; Chambers, C. C.; Giesen, D. J.; Liotard, D. A.; Cramer, C. J.; Truhlar, D. G. *ACS Symp. Ser.* **1998**, *712*, 201–219.
132. Klamt, A. *COSMO-RS: From Quantum Chemistry to Fluid Phase Thermodynamics and Drug Design*; Elsevier Science Ltd.: Amsterdam, the Netherlands, 2005.
133. Klamt, A.; Jonas, V.; Burger, T.; Lohrenz, J. C. W. *J. Phys. Chem. A* **1998**, *102*, 5074–5085.
134. Ben-Naim, A. *Statistical Thermodynamics for Chemists and Biochemists*; Plenum: New York, 1992; p. 421ff.
135. Uudsemaa, M.; Tamm, T. *J. Phys. Chem. A* **2003**, *107*, 9997–10003.
136. Jaque, P.; Marenich, A. V.; Cramer, C. J.; Truhlar, D. G. *J. Phys. Chem. C* **2007**, *111*, 5783–5799.
137. Ho, J.; Klamt, A.; Coote, M. L. *J. Phys. Chem. A* **2010**, *114*, 13442–13444.
138. Ribeiro, R. F.; Marenich, A. V.; Cramer, C. J.; Truhlar, D. G. *J. Phys. Chem. B* **2011**, *115*, 14556.
139. Hünenberger, P.; Reif, M. *Single-Ion Solvation: Experimental and Theoretical Approaches to Elusive Thermodynamic Quantities*; RSC Publishing: Cambridge, U.K., 2011.
140. Fawcett, W. R. *Langmuir* **2008**, *24*, 9868–9875.
141. Sokhan, V. P.; Tildesley, D. J. *Mol. Phys.* **1997**, *92*, 625–640.
142. Randles, J. E. B. *Phys. Chem. Liq.* **1977**, *7*, 107–179.
143. Kathmann, S. M.; Kuo, I.-F. W.; Mundy, C. J. *J. Am. Chem. Soc.* **2008**, *130*, 16556–16561.
144. Kelly, C. P.; Cramer, C. J.; Truhlar, D. G. *J. Phys. Chem. B* **2006**, *110*, 16066–16081.
145. Tissandier, M. D.; Cowen, K. A.; Feng, W. Y.; Gundlach, E.; Cohen, M. H.; Earhart, A. D.; Coe, J. V.; Tuttle, Jr., T. R. *J. Phys. Chem. A* **1998**, *102*, 7787–7794.
146. Donald, W. A.; Demireva, M.; Leib, R. D.; Aiken, M. J.; Williams, E. R. *J. Am. Chem. Soc.* **2010**, *132*, 4633–4640.
147. Donald, W. A.; Leib, R. D.; Demireva, M.; O'Brien, J. T.; Prell, J. S.; Williams, E. R. *J. Am. Chem. Soc.* **2009**, *131*, 13328–13337.

148. Donald, W. A.; Leib, R. D.; O'Brien, J. T.; Williams, E. R. *Chem. Eur. J.* **2009**, *15*, 5926–5934.
149. Barone, V.; Cossi, M.; Tomasi, J. J. *Chem. Phys.* **1997**, *107*, 3210–3221.
150. Gritzner, G.; Kuta, J. *Pure Appl. Chem.* **1984**, *4*, 462–466.
151. Namazian, M.; Lin, C. Y.; Coote, M. L. *J. Chem. Theory Comput.* **2010**, *6*, 2721–2725.
152. Fu, Y.; Liu, L.; Li, R.-Q.; Liu, R.; Guo, Q.-X. *J. Am. Chem. Soc.* **2004**, *126*, 814–822.
153. Marcus, R. A. *Annu. Rev. Phys. Chem.* **1964**, *15*, 155–196.
154. Marcus, R. A. *J. Chem. Phys.* **1956**, *24*, 966–978.
155. Li, J.; Cramer, C. J.; Truhlar, D. G. *Int. J. Quant. Chem.* **2000**, *77*, 264–280.
156. Marenich, A. V.; Cramer, C. J.; Truhlar, D. G.; Guido, C. A.; Mennucci, B.; Scalmani, G.; Frisch, M. J. *Chem. Sci.* **2011**, *2*, 2143–2161.
157. Frisch, M. J.; Trucks, G. W.; Schlegel, H. B.; Scuseria, G. E.; Robb, M. A.; Cheeseman, J. R.; Scalmani, G.; Barone, V.; Mennucci, B.; Petersson, G. A.; Nakatsuji, H.; Caricato, M.; Li, X.; Hratchian, H. P.; Izmaylov, A. F.; Bloino, J.; Zheng, G.; Sonnenberg, J. L.; Hada, M.; Ehara, M.; Toyota, K.; Fukuda, R.; Hasegawa, J.; Ishida, M.; Nakajima, T.; Honda, Y.; Kitao, O.; Nakai, H.; Vreven, T.; Montgomery, Jr., J. A.; Peralta, J. E.; Ogliaro, F.; Bearpark, M.; Heyd, J. J.; Brothers, E.; Kudin, K. N.; Staroverov, V. N.; Kobayashi, R.; Normand, J.; Raghavachari, K.; Rendell, A.; Burant, J. C.; Iyengar, S. S.; Tomasi, J.; Cossi, M.; Rega, N.; Millam, N. J.; Klene, M.; Knox, J. E.; Cross, J. B.; Bakken, V.; Adamo, C.; Jaramillo, J.; Gomperts, R.; Stratmann, R. E.; Yazyev, O.; Austin, A. J.; Cammi, R.; Pomelli, C.; Ochterski, J. W.; Martin, R. L.; Morokuma, K.; Zakrzewski, V. G.; Voth, G. A.; Salvador, P.; Dannenberg, J. J.; Dapprich, S.; Daniels, A. D.; Farkas, Ö.; Foresman, J. B.; Ortiz, J. V.; Cioslowski, J.; Fox, D. J. *Gaussian 09*, Revision A.1; Gaussian, Inc.: Wallingford, CT, 2009.
158. MOLPRO version 2009.1 is a package of ab initio programs written by Werner, H.-J.; Knowles, P. J.; Lindh, R.; Manby, F. R.; Schütz, M.; Celani, P.; Korona, T.; Mitrushenkov, A.; Rauhut, G.; Adler, T. B.; Amos, R. D.; Bernhardsson, A.; Berning, A.; Cooper, D. L.; Deegan, M. J. O.; Dobbyn, A. J.; Eckert, F.; Goll, E.; Hampel, C.; Hetzer, G.; Hrenar, T.; Knizia, G.; Köppl, C.; Liu, Y.; Lloyd, A. W.; Mata, R. A.; May, A. J.; McNicholas, S. J.; Meyer, W.; Mura, M. E.; Nicklaß, A.; Palmieri, P.; Pflüger, K.; Pitzer, R.; Reiher, M.; Schumann, U.; Stoll, H.; Stone, A. J.; Tarroni, R.; Thorsteinsson, T.; Wang, M.; Wolf, A. University College Cardiff Consultants Limited: Cardiff, Wales, 2009.
159. Goldstein, S.; Samuni, A.; Hideg, K.; Meranyi, G. *J. Phys. Chem. A* **2006**, *110*, 3679–3685.
160. Ilan, Y.; Czapski, G.; Meisel, D. *Biochim. Biophys. Acta* **1976**, *430*, 209–224.
161. Isse, A. A.; Lin, C. Y.; Coote, M. L.; Gennaro, A. *J. Phys. Chem. B* **2011**, *115*, 678–684.
162. Isse, A. A.; Sandona, G.; Durante, C.; Gennaro, A. *Electrochim. Acta* **2009**, *54*, 3235–3243.
163. Camaioni, D. M.; Schwerdtfeger, C. A. *J. Phys. Chem. A* **2005**, *109*, 10795–10797.
164. Zare, H. R.; Eslami, M.; Namazian, M.; Coote, M. L. *J. Phys. Chem. B* **2009**, *113*, 8080–8085.
165. Kennedy, J. A.; Munro, M. H. G.; Powel, H. K. J.; Porter, L. J.; Foo, L. Y. *Aust. J. Chem.* **1984**, *37*, 885–892.